

LUDWIG-MAXIMILIANS-UNIVERSITÄT
MÜNCHEN

BACHELOR'S THESIS

Setup and characterization of a Littrow laser
for 689 nm

Lukas Homeier

in collaboration with *Max-Planck-Institute for Quantum Optics*
under supervision of Prof. Dr. Immanuel Bloch and Dr. Sebastian Blatt

Munich, 2017



LUDWIG-MAXIMILIANS-UNIVERSITÄT
MÜNCHEN

**Aufbau und Charakterisierung eines Littrow
Lasers für 689 nm**

Bachelorarbeit an der Fakultät für Physik
vorgelegt von Lukas Homeier

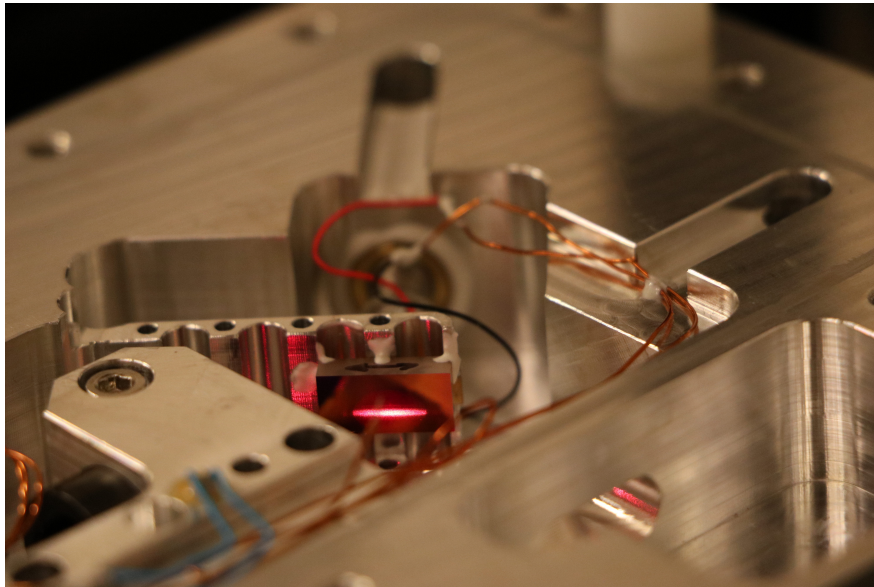
München, am 03. Juli 2017



Für Opa

Abstract

Atomic physics experiments with ultracold matter require stable and narrow-linewidth lasers. In this ten-week Bachelor's project a tunable diode laser in Littrow configuration [1] for cooling and trapping strontium atoms at 689 nm was assembled, optimized and characterized. In the beginning, I discuss the theory of lasers with special focus on semiconductor laser diodes as well as blazed diffraction gratings to understand the Littrow and Littman design. Moreover, I report on the setup of my laser system and explain a PID temperature controller and its optimization to achieve long-term stability. To maximize the fiber coupling efficiency, the mode of the beam is shaped with an anamorphic prism pair for which a formula in ray optics is derived. For continuously scanning the laser's frequency, the current is coupled to a feed-forward controller and a mode-hop-free tuning range of (15.3 ± 0.05) GHz was obtained by observation with a confocal cavity. At last, the laser's linewidth is measured by the transmission through a cavity as well as by the analysis of a heterodyne beatnote signal. From the latter technique a linewidth at Full Width at Half Maximum (FWHM) of $\Delta\nu = (127.8 \pm 14.4)$ kHz for a measurement time of $T = 100 \mu\text{s}$ results. The project was done in the group of Prof. Dr. Immanuel Bloch under supervision of Dr. Sebastian Blatt in the new strontium lab at the MPQ.



Contents

Abstract	ii
1 Introduction	1
2 Laser	3
2.1 Fundamental Processes of Light-Atom Interaction	3
2.2 Light Amplification	6
2.3 Laser Oscillations	8
2.4 Semiconductor Laser Diodes	9
2.4.1 Semiconductors in a p-i-n junction	9
2.4.2 Output Power of Laser Diodes	12
2.5 Gratings	14
2.5.1 Grating in the Fraunhofer Approximation	15
2.5.2 Blazed Gratings	17
2.6 Laser Designs	19
2.6.1 Littrow Configuration	20
2.6.2 Littman Configuration	21
2.6.3 Littrow vs. Littman Laser	21
3 Design and Setup	23
3.1 Mechanical Design	23
3.2 Sonication	25
3.3 Brewster Window	26
3.4 Temperature Control Elements	26
3.5 Electronic Circuit	27
3.5.1 D-Sub 9 Connection	27
3.5.2 Protection Board	28
3.6 The Laser Diode and Collimation Tube	29
3.7 The Grating	31
3.8 Aligning to Feedback	32
3.9 Optimization	33
3.9.1 Minimizing Threshold Current	33
3.9.2 PID-Controller	34

4	Optical setup	39
4.1	General Features	40
4.2	Anamorphic Prism Pair	41
5	Performance of the Laser	47
5.1	Mode-Hop-free Tuning Range	47
5.1.1	Optical Resonators and Gaussian Beams	47
5.1.2	Optimization of the Mode-Hop-free Tuning Range	51
5.2	Linewidth	55
5.2.1	Linewidth Measurement with a Cavity	55
5.2.2	Heterodyne Linewidth Measurement	57
6	Conclusion	63
	Acknowledgments	65
	Bibliography	67
	Appendix	71
A	Calculations for Chapter 2.5	71
B	Protection Circuit	72
C	Magnification Factor of an Anamorphic Prism Pair	75

List of Figures

2.1	Light-atom interaction	4
2.2	Light amplification by stimulated emission	6
2.3	Gain and losses in an optical resonator	9
2.4	The valence and conduction band in a semiconductor	10
2.5	A semiconductor p-i-n junction in steady-state	11
2.6	A semiconductor p-i-n junction with forward bias applied	12
2.7	Threshold current measurement	14
2.8	Angle convention for gratings	15
2.9	Illustration for Fraunhofer diffraction	16
2.10	Shape of a blazed grating	18
2.11	The effect of the blaze angle on the intensity pattern	19
2.12	Littrow configuration	20
2.13	Littman configuration	21
3.1	Implementation of the Littrow configuration	23
3.2	Mechanical drawing of the Littrow design	24
3.3	Orientation of the Peltier elements	27
3.4	Pin connection of the D-Sub 9 plug	28
3.5	Pin connection of the laser diode	30
3.6	The dimensions of the collimation tube and aspherical lens	31
3.7	Critical oscillation of a proportional feedback controller	35
3.8	Response signal of the PI-controller	36
3.9	Response signal of the PID-controller	37
4.1	The optical setup for fiber coupling	39
4.2	Angle convention for the anamorphic prism pair	42
4.3	Magnification and diffraction of an anamorphic prism pair	43
4.4	The beam profile of the laser without shaping	43
4.5	The beam profile of the laser after shaping	44
5.1	The Finesse of a Fabry-Pérot-Etalon for different reflectivities	49
5.2	Illustration of a confocal cavity	51
5.3	The reason of mode-hops	52
5.4	Optical setup for mode-matching with a confocal cavity	53

5.5	Alignment of a confocal cavity	54
5.6	Transmission of the home-built laser through a confocal cavity . .	56
5.7	Transmission of a reference laser through a confocal cavity	57
5.8	Optical setup for the beatnote measurement	59
5.9	The beatnote signal	60
5.10	Evaluation of the Power Spectral Density for $T = 100 \mu s$	61
B.1	The protection circuit page 1/2.	73
B.2	The protection circuit page 2/2	74

Chapter 1

Introduction

Since the invention of the first laser in 1960 [2], it has found many applications in daily life. A manifold of technologies are based on lasers and many people think of treatments in medicine, the CD-ROM, stage lighting or optical communication. But this source of light is also an essential instrument in physics research where we can make use of its precision for cooling of atomic clouds [3, 4]. In the field of ultracold quantum gases, matter is cooled down to almost absolute zero such that the motion of the atoms freezes out. With the development of further cooling techniques, temperatures can be reached at which a phase transition occurs and the gas is forming a new state of matter called Bose-Einstein Condensate (BEC) [5]. This means that the atoms - which are described by waves in terms of quantum mechanics - start to oscillate synchronously instead of moving randomly. Because we have a cloud containing several thousands to millions of atoms which all behave the same, we can detect their quantum behavior merely by imaging them with a camera. With this method, the tiny scale of quantum nature is enlarged to macroscopic dimensions. But we can go even further. Since we have an instrument that allows us to observe the quantum effects of many atoms, structures found in nature can be imitated, for instance, the periodic structure of solid matter. These periodic structures are again created by laser light that forms a standing wave, called optical lattice, in which the BEC can be loaded [6]. With the atoms in the optical lattice, we can learn how the interaction of many particles work on the level of quantum mechanics [7].

Strontium is the element that *we* use to implement an optical lattice loaded with ultracold atoms. Strontium as an alkaline-earth element has two valence electrons and gives us a rich energy structure. It allows us to experiment with a variety of lattice potentials that can be loaded with bosonic and fermionic isotopes simultaneously and the atom also features a very narrow “clock-transition” for precise measurements in the lattice. To address all the transitions of importance, different kinds of lasers are required that have to work stably and reliably. One stage of the cooling procedure to reach a BEC, is done in a magneto-optical trap (MOT) with the specific transition $5s^2\ ^1S_0 \rightarrow 5s5p\ ^3P_1$ at 689 nm [8]. This thesis

reports on the setup of a tunable diode laser that can be used for the red MOT transition.

Chapter 2

Laser

Lasers play an important role both in research and in technical applications. In this chapter we give an overview of laser physics and discuss semiconductor laser diodes as well as diffraction gratings, which are part of the Littrow laser design that I implemented. These Littrow lasers feature tunability of the wavelength and are described in detail at the end of this chapter.

2.1 Fundamental Processes of Light-Atom Interaction

LASER is an acronym for *Light Amplification by Stimulated Emission of Radiation*. The physical effect of stimulated emission was first predicted by Albert Einstein in 1916 [9]. Let us assume that we have an electron in a non-degenerate two-level system with eigenstates $|1\rangle$ and $|2\rangle$, and associated energies E_1 and E_2 , respectively. The energy difference is given by $\Delta E = E_2 - E_1 > 0$ as shown in Fig. 2.1. If we consider an ensemble of such two-level systems, where each system contains a single electron, the number of systems with an electron in $|1\rangle$ ($|2\rangle$) is N_1 (N_2) and the total number of two-level systems is $N = N_1 + N_2$. Moreover, photons with energies $E_{\text{ph}} = \Delta E = \hbar\omega_{21}$ can interact with each two-level system, where \hbar is the Planck constant divided by 2π and ω_{21} is the angular frequency of the light field. The spectral energy density of the light field is defined as $\rho(\omega_{21})$. The interactions can be classified into three processes [10]:

1. **Absorption** of photons: an electron in state $|1\rangle$ can absorb a photon of energy $\hbar\omega_{21}$ and thereby change its state to the excited state $|2\rangle$ (see Fig. 2.1a). The transition rate is proportional to the population of the ground state N_1 , the energy density $\rho(\omega_{21})$ of the light field and a proportionality constant $B_{12} > 0$, the so-called Einstein B -coefficient, and thus $\dot{N}_1 = N_1 B_{12} \rho(\omega_{21})$.
2. **Spontaneous emission**: an electron in state $|2\rangle$ can change its state spontaneously to state $|1\rangle$ by emitting a photon of energy $\hbar\omega_{21}$. The emitted

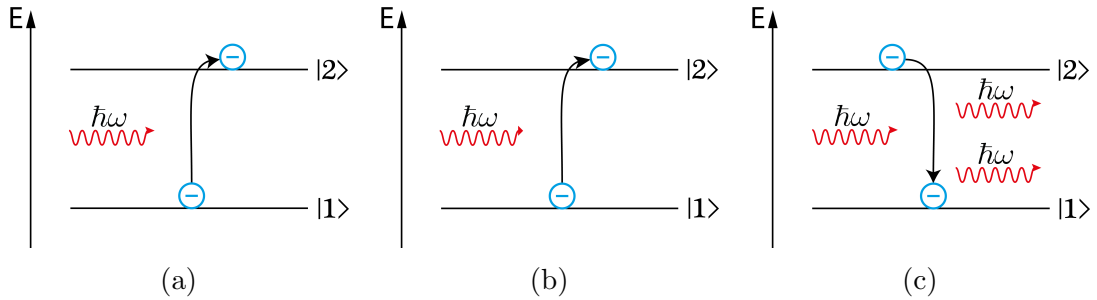


Figure 2.1: The energy difference between the excited and ground state is given by $\Delta E = \hbar\omega_{21}$. Panel (a) shows the absorption of a photon and excitation of the electron. In Panel (b), we sketch the spontaneous emission of a photon so that the electron falls into the ground state. In Panel (c) an incoming photon is shown that stimulates the emission of an indistinguishable photon.

photon has a random direction, orientation of polarization, and phase (see Fig. 2.1b). If we look at N_2 systems, the rate of decay is simply described by $\dot{N}_2 = -A_{21}N_2$, with $A_{21} > 0$, where the subscript indicates the decay from $|2\rangle \rightarrow |1\rangle$. Here, A_{21} is the so-called Einstein A -coefficient. The minus sign shows that the population N_2 shrinks over time. The solution is an exponential decay $N_2(t) = N_{2,0} \exp(-A_{21}t)$, where t is the time and $N_{0,2} = N_2(t = 0)$. Therefore we can define $\tau_{21} := \frac{1}{A_{21}}$ as the lifetime of state $|2\rangle$ and after $t = \tau_{21}$ the population of N_2 has decreased by a factor of $\frac{1}{e}$. The lifetime of a state is also of physical significance in experiments for systems with more than two levels.

- 3. Stimulated emission:** an electron in state $|2\rangle$ can not only move to state $|1\rangle$ by a spontaneous process but can also be forced to change into the ground state $|1\rangle$ by interaction with a photon. When a photon with energy $\hbar\omega_{21}$ interacts with an electron in state $|2\rangle$, the electron is afterwards in state $|1\rangle$ and an additional photon with energy $\hbar\omega_{21}$ is produced with the same direction, orientation of polarization, and phase as the incident photon (see Fig. 2.1c). We say that these two photons are coherent. In this process the light field is amplified. In analogy to the absorption process the transition rate is given by $\dot{N}_2 = N_2 B_{21} \rho(\omega_{21})$.

To derive a relation between the constants B_{12} , B_{21} and A_{21} , we apply the Principle of Detailed Balance [9]. The system should now be in thermal equilibrium with the interacting radiation field. In the equilibrium state, the process of photons changing from $|1\rangle \rightarrow |2\rangle$ should balance the inverse process $|2\rangle \rightarrow |1\rangle$, so that

$$N_1 B_{12} \rho(\omega_{21}) = N_2 B_{21} \rho(\omega_{21}) + A_{21} N_2 \quad (2.1a)$$

$$\iff \rho(\omega_{21}) = \frac{A_{21}/B_{21}}{\frac{N_1 B_{12}}{N_2 B_{21}} - 1}. \quad (2.1b)$$

To derive an expression for the ratio N_1/N_2 , we make use of thermodynamics. In terms of statistical physics, we consider a canonical assemble of two-level systems with energy eigenstates E_1 and E_2 . The probability of a non-degenerate two-level system being in state $|i\rangle$ ($i = 1, 2$) is given by

$$P_i(T) = \frac{\exp\left(-\frac{E_i}{k_B T}\right)}{\sum_{i=1}^2 \exp\left(-\frac{E_i}{k_B T}\right)}, \quad (2.2)$$

where k_B is the Boltzmann constant and T is the temperature.

From Eqn. (2.2), the ratio of systems in the excited and in the ground state can be determined as

$$\frac{N_1}{N_2} = \frac{N \cdot P_1}{N \cdot P_2} = \frac{\exp\left(-\frac{E_1}{k_B T}\right)}{\exp\left(-\frac{E_2}{k_B T}\right)} = \exp\left(\frac{\hbar\omega_{21}}{k_B T}\right) \geq 1. \quad (2.3)$$

The inequality holds because the argument of the exponential function is always positive, and it shows that in thermal equilibrium the population in the ground level is always greater than in the excited state.

Inserting now Eqn. (2.3) into Eqn. (2.1b) gives a relation between the energy density and properties of the two-level system, i.e. the Einstein coefficients, the temperature and the system's energetic structure

$$\rho(\omega_{21}) = \frac{A_{21}/B_{21}}{\frac{B_{12}}{B_{21}} \exp\left(\frac{\hbar\omega_{21}}{k_B T}\right) - 1}. \quad (2.4)$$

Now we use Planck's law which describes the energy density of blackbody radiation in a frequency interval $[\omega, \omega + d\omega]$ in thermal equilibrium:

$$\rho(\omega)d\omega = \frac{\hbar\omega^3}{\pi^2 c^3} \frac{1}{\exp\left(\frac{\hbar\omega}{k_B T}\right) - 1} d\omega, \quad (2.5)$$

where c is the speed of light.

In the last step we compare the coefficients of Eqns. (2.4) and (2.5) get the **Einstein relations**:

$$B_{12} = B_{21} \quad (2.6a)$$

$$\frac{A_{21}}{B_{21}} = \frac{\hbar\omega_{21}^3}{\pi^2 c^3} \quad (2.6b)$$

These relations show that the two-level system does not differentiate between absorption and stimulated emission of photons which happen with the same rate

for the same population. Also, in the postulates of the transition probabilities the Einstein A/B -coefficients were assumed to be constants for a specific system and independent of the radiation field. We derived the Einstein relations Eqn. (2.6) for interaction with blackbody radiation and obtained an expression for the relation between the A/B -coefficients. Since the coefficients are constants, we can calculate the transition rates of the populations for arbitrary radiation fields, i.e. also for fields that are not given by blackbody radiation.

2.2 Light Amplification

We would like to consider what happens to a beam of radiation that travels through a medium consisting of two-level systems. This will allow us to derive a necessary condition for light amplification.

Up to now we discussed two-level systems, where the energy levels have a fixed energy difference. But if we think of quantum mechanics, effects of uncertainty come up. This means that the energy difference is not given by an exact value but becomes diffuse. That is why we have to introduce a new function $g(\omega)\delta\omega$ to our transition rate which then reads $\dot{N}_i = N_i B_{21} \rho(\omega_{21}) g(\omega) \delta\omega$. This additional function determines the ability of our two-level system to interact with photons of angular frequency in the interval $[\omega, \omega + \delta\omega]$, even if they do not have energy $\hbar\omega_{21}$. This function describes the so-called linewidth of a transition and is usually a lorentzian function with the maximum at $\omega = \omega_{21}$.

A beam enters a section A of a medium with a certain intensity $\mathcal{I}(z)$ and leaves the medium after a distance δz with intensity $\mathcal{I}(z + \delta z)$ as shown in Fig. 2.2.

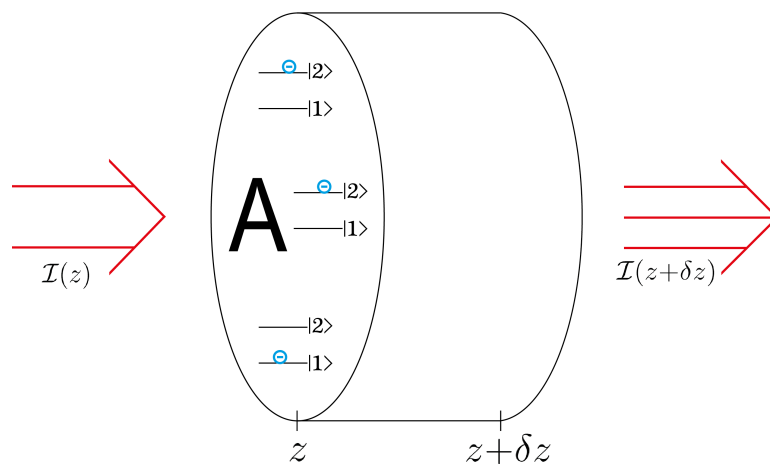


Figure 2.2: A beam travels through a medium of two-level systems of volume $A \cdot \delta z$. Depending on the sign of $(N_2 - N_1)$ the beam is either amplified or damped.

The change of energy in the beam per time in a frequency interval is given by the change of photon number in the beam, multiplied by the photon energy. Without spontaneous emission, this energy change is given by

$$(n_2 - n_1)B_{21}g(\omega)\frac{\mathcal{I}(z)}{c}A\delta z \cdot \hbar\omega_{21}, \quad (2.7)$$

where $n_i = \frac{N_i}{A\delta z}$ ($i = 1, 2$) is the population density of state $|i\rangle$. Moreover, we used the Einstein relation, Eqn. (2.6), and $\mathcal{I}(z) := \mathcal{I}(\omega_{21}, z) = \rho(\omega_{21}, z)\delta\omega \cdot c$. Here $\rho(\omega_{21}, z)\delta\omega$ is the energy density in the angular frequency interval $[\omega_{21}, \omega_{21} + \delta\omega]$ and at spatial position z .

If we would like to calculate the difference in energy per time by a change of intensity, we have to consider

$$\left[\mathcal{I}(z + \delta z) - \mathcal{I}(z)\right]A = \left[\mathcal{I}(z) + \frac{\partial\mathcal{I}}{\partial z}\delta z + \dots - \mathcal{I}(z)\right]A \approx \frac{\partial\mathcal{I}(z)}{\partial z}\delta z A, \quad (2.8)$$

for an infinitesimal interval $\delta z \rightarrow 0$. Now equating Eqns. (2.7) and (2.8) gives

$$\frac{\partial\mathcal{I}(z)}{\partial z} = (n_2 - n_1)B_{21}g(\omega)\frac{\mathcal{I}(z)}{c}\hbar\omega_{21}, \quad (2.9)$$

which can be solved easily:

$$\mathcal{I}(z) = \mathcal{I}_0 \exp\left[(n_2 - n_1)B_{21}g(\omega)\frac{\hbar\omega_{21}}{c}z\right] = \mathcal{I}_0 \exp(\alpha_g z). \quad (2.10)$$

Here $\mathcal{I}_0 := \mathcal{I}(z = 0)$ is an integration constant and $\alpha_g := (n_2 - n_1)B_{21}g(\omega)\frac{\hbar\omega_{21}}{c}$ is the so-called gain coefficient. As you can see from Eqn. (2.10), the intensity only increases if $\alpha_g > 0$ or, because both B_{21} and $\hbar\omega_{21}$ are positive quantities, if

$$n_2 - n_1 > 0 \Leftrightarrow N_2 - N_1 > 0. \quad \textbf{(Condition for optical gain)} \quad (2.11)$$

Thus the incoming beam can be amplified only if there are more systems with electrons in the excited state than in the ground state. This situation is called population inversion. The condition for optical gain can be understood in a very descriptive picture. A photon traveling through a medium is either absorbed or copied (or nothing happens). If the possibility for creating coherent photons is greater than for absorbing photons, the beam is amplified.

Let us again reformulate the equilibrium state Eqn. (2.1a) and insert the Einstein relations Eqn. (2.6):

$$\frac{N_1}{N_2} = \frac{B_{21}\rho(\omega_{21}) + A_{21}}{B_{21}\rho(\omega_{21})} = 1 + \frac{\hbar\omega_{21}^3}{\pi^2 c^3 \rho(\omega_{21})} > 1. \quad (2.12)$$

Hence, we see that for a two-level system interacting with radiation the population always obeys $N_1 > N_2$. So in a two-level system, we can reach a steady-state

population inversion neither by interaction with light nor by thermal excitation as discussed in the previous section. To reach the regime of population inversion then, the medium has to be pumped by a process that can excite electrons and is not limited to $N_1 > N_2$. Because this can not be done in a two-level system, different techniques have been developed, e.g. by using a third energy level. How pumping works in semiconductor laser diodes is explained later in Ch. 2.4.

2.3 Laser Oscillations

In the previous section, a condition for amplifying light was found: the population inversion. If we have a pumped medium with population inversion (a gain medium), it would indeed emit radiation because photons of spontaneous emission are amplified. But because these photons are created at random positions in the gain medium and travel in random directions, the radiation is not coherent and the energy is not focused into a small spatial angle. Shortly, this is not what we would call a laser. We desire to have a laser that emits coherent light. Thus, the gain medium has to interact with indistinguishable photons and not with random photons. That is why we have to put the gain medium between two mirrors, a so called cavity or optical resonator. In this case, the photons do not just leave the gain medium and a different, randomly emitted photon is amplified and then leaves the gain medium again. Instead, coherent photons are reflected back into the gain medium and by stimulated emission a defined light field with indistinguishable photons is created within the cavity.

Resonators will be discussed in detail later, here we would like to consider the interaction of light and the gain medium in a cavity. Let us assume two planar mirrors with intensity reflectivity R_1 and R_2 , respectively, that are mounted parallel at a distance d with a gain medium of length l_g in between (see Fig. 2.3). The intensity of a beam that propagates once back and forth in the gain medium, is amplified by $\mathcal{I}(2l_g) = \mathcal{I}_0 \exp(2\alpha_g l_g)$ [Eqn. (2.10)]. Moreover, we have losses due to finite reflectivities, spontaneous emission and other scattering events, e.g. phonon excitation. These losses can again be described as a decay rate and therefore the intensity of the beam after one round trip in the cavity without gain medium is $\mathcal{I}(2d) = \mathcal{I}_0 R_1 R_2 \exp(-2\alpha_\ell d)$, where $\alpha_\ell > 0$ is a loss coefficient. The condition for laser oscillations to occur is now that gain equals the losses in the resonator, hence that a light field in the resonator does not decay [11, 12]:

$$R_1 R_2 \exp(-2\alpha_\ell d) = \exp(-2\alpha_g l_g) \quad (\text{Threshold condition}) \quad (2.13)$$

Because the left side of the equation is fixed by the properties of the cavity, a laser fulfills the threshold condition as soon as $\alpha_g \propto N_2 - N_1$ is large enough to balance the losses. In a semiconductor laser diode, for example, one can increase the pumping rate and thus α_g by increasing the current in the gain medium.

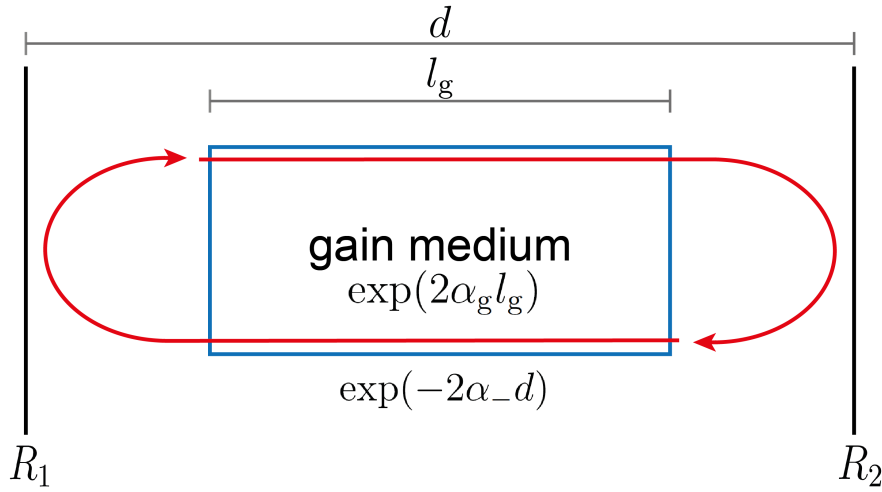


Figure 2.3: Two planar mirrors at distance d form a resonator. The red arrows indicate a beam of light that is reflected on the mirrors and travels back and forth in the cavity. Moreover the pumped gain medium of length l_g can lead to non-decaying oscillations of light, if it can compensate for the losses of the cavity.

2.4 Semiconductor Laser Diodes

In this chapter we would like to consider lasers based on a semiconductor gain medium. They are widely spread because of their small size, simple pumping by applying current and their long lifetime of more than 100 000 h. Here I will qualitatively present the idea of how a semiconductor laser diode works. For further reading, Refs. [11–13] are recommended. First, I would like to give a short overview of semiconductors and how to create regions of population inversion. Then we use the knowledge from the preceding chapters about lasers and apply it to semiconductor laser diodes to determine the output power.

2.4.1 Semiconductors in a p-i-n junction

The situation of two-level systems described in Ch. 2.1 does not hold anymore in semiconductors. In semiconductors the energy states combine to energy bands [14, 15]. These bands are divided into the valence band and the conduction band and are separated in energy by the so-called band gap with gap energy E_g . Since the number of states in a band is finite and each state can (due to Pauli's exclusion principle) be occupied just by two electrons, the maximum number of electrons in a band is limited. If the band is completely occupied, electrons cannot move freely within the band, whereas vacant states in the band allow electrons to move. Usually the valence band of a solid state is completely occupied, while the conduction band has vacant places. This is what the name conduction band

derives from.

At $T = 0$ the valence band of a semiconductor is indeed completely occupied by electrons, while the conduction band is vacant. So at $T = 0$ a semiconductor is an electric insulator. By increasing the temperature, the probability for electrons to be in the conduction band also increases, because the gap energy is small enough that electrons can overcome it by thermal excitation. Thus, for $T > 0$ a semiconductor gets conductive, however the conductivity is much less than that of a usual conductor such as copper. Moreover, a property of a semiconductor is the Fermi energy E_F . It describes the energy that is required to add an additional electron to the solid at temperature $T = 0$. For semiconductors E_F is within the band gap as shown in Fig. 2.4 and an electron that is added will therefore appear in the conduction band.

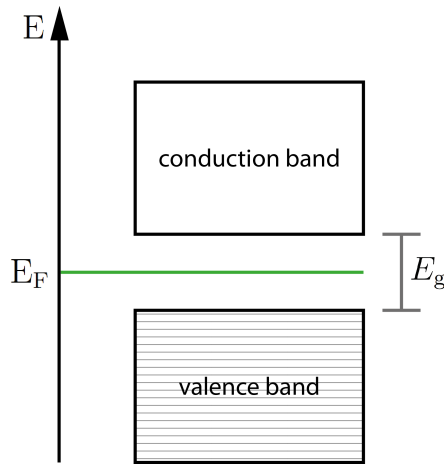


Figure 2.4: A sketch of the energy distribution of the valence and conduction bands in a semiconductor. The Fermi energy is in the middle of the gap that has an energetic width E_g . For $T = 0$, the valence band is completely occupied while the conduction band is empty.

The absence of an electron in the valence band is called a hole and can be described by a positive charge. The process of stimulated emission is not only dependent on the population of electrons in the conduction band but also on the population of holes in the valence band. A region where we can have a population inversion, in the sense of higher probability to have stimulated emission than absorption, can be realized by a p-i-n junction. This means a conjunction of a p-doped, an intrinsic and a n-doped semiconductor in this order (see Fig. 2.5). A p-doped semiconductor is a semiconductor material, where atoms from a different element are added so that the density of holes increases in the valence band. In contrast, a n-doped semiconductor has a higher density of electrons in the conduction band than an intrinsic one that simply stands for the pure semiconductor element. If now the p-i-n junction is formed, a spatial gradient

of holes and electrons is created. In Fig. 2.5 the region shown on left side of the figure has a high density of holes and a low density of electrons, where the right side has the inverse densities. This density gradient leads to diffusion of holes and electrons at the junction until a steady-state is reached. This gradient can also be expressed by a difference in the Fermi energy E_F of the p-doped, intrinsic and n-doped semiconductor. The charges flow until the Fermi energies are equal. Thus, negative charges collect on the p-doped side and positive charges on the n-doped side so that an internal electric field results.

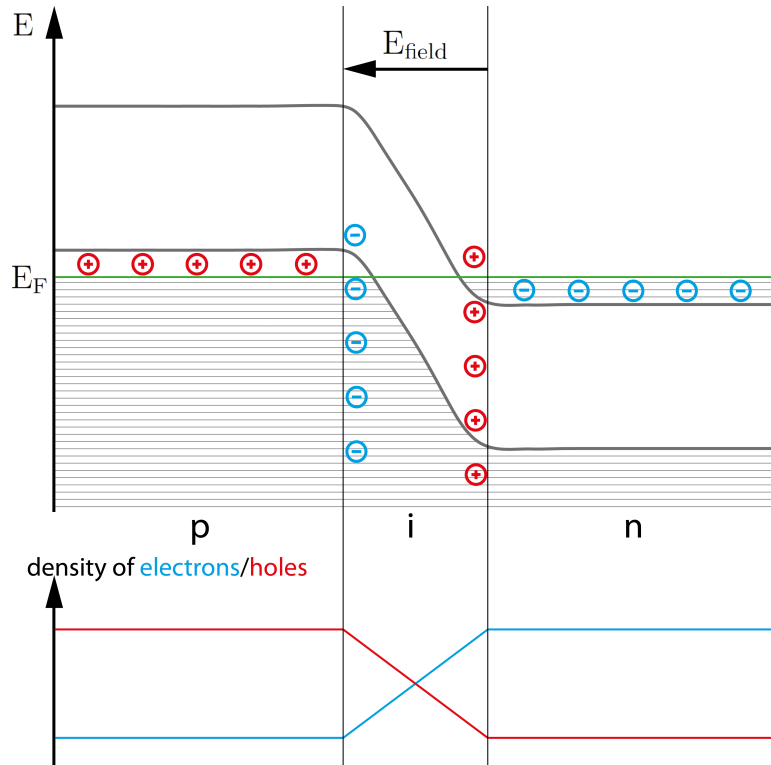


Figure 2.5: The energy band structure for a p-i-n junction. The lower band is the valence band and the upper one is the conduction band. In between is an energy gap. The dashed area indicates an occupation of electrons. Because of different densities of holes and electrons on the left and right side of the junction, an internal electric field is created in the intrinsic region by diffusion of charges.

Let us now apply a forward bias voltage, that means a higher potential on the p-doped side and lower potential on the n-doped side. Then our system is perturbed and the Fermi energy is divided into the Fermi energy for the valence band of the p-doped semiconductor E_{F_v} and into the Fermi energy for the conduction band of the n-doped semiconductor E_{F_c} as shown in Fig. 2.6.

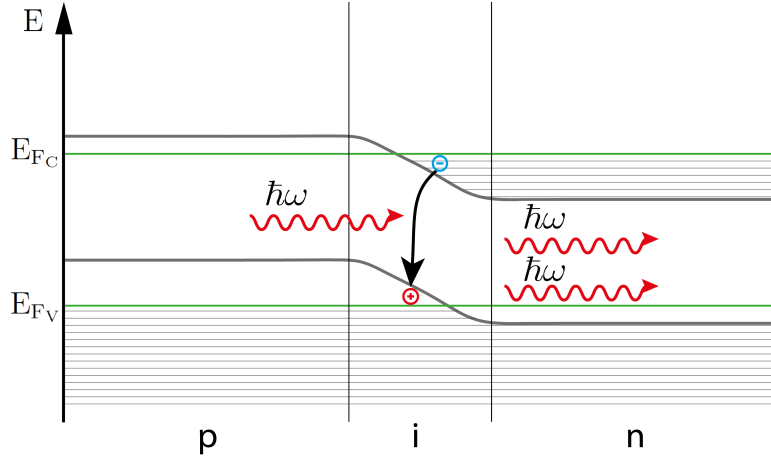


Figure 2.6: The band structure of a p-i-n junction as in Fig. 2.5 but with an anode connected to the left side and ground on the right side. The energy gradient between the energy bands of the p- and n-doped semiconductors decreases in such a way that a region of population inversion is created in the area of the intrinsic semiconductor. A photon with the energy of the band gap can stimulate an electron-hole-recombination and a coherent photon is emitted.

Hence, by applying voltage in this direction we compensate the internal electrical field such that the electron from the conduction band of the n-doped side can overcome the potential barrier and a current flows. Now we are able to understand how population inversion occurs in this p-i-n junction. The external potential changes the energy bands and an overlap region is created, with both electrons in the conduction band and holes in the valence band. This was our condition for stimulated emission in the beginning of this chapter. An incident photon with energy $E_{\text{ph}} = \hbar\omega_{\text{cv}} := E_{F_C} - E_{F_V}$ can now stimulate the system to an electron-hole-recombination and a coherent photon is emitted.

2.4.2 Output Power of Laser Diodes

As we know from Ch. 2.3, the gain coefficient α_g and thus the population inversion has to be large enough to balance the losses in the resonator. The reflective sides of the resonator in a semiconductor laser diode are usually formed by the edge of the semiconductor junction itself. The difference in refractive index between the semiconductor and the surrounding gas leads to reflectivities large enough to form a cavity for the laser diode [11].

The gain medium has dimensions of a few ten to few hundred micrometers. That is why we can approximate the increase of intensity after the beam travels back and forth through the gain medium with length l_g by Eqn. (2.10),

$$\mathcal{I}(2l_g) = \mathcal{I}_0 \exp(2\alpha_g l_g) \approx \mathcal{I}_0(1 + 2\alpha_g l_g) \Leftrightarrow \mathcal{I}(2l_g) - \mathcal{I}_0 \approx 2\alpha_g l_g. \quad (2.14)$$

Thus, if we consider gain media where $2\alpha_g l_g \ll 1$ even for several round trips, the output power P of the laser grows linearly in the gain coefficient α_g . The same argument can be used for the losses within the cavity of length d and $2\alpha_\ell d \ll 1$:

$$\mathcal{I}(2d) = \mathcal{I}_0 \exp(-2\alpha_\ell d) \approx \mathcal{I}_0(1 - 2\alpha_\ell d) \Leftrightarrow \mathcal{I}(2d) - \mathcal{I}_0 \approx -2\alpha_\ell d \quad (2.15)$$

In semiconductor laser diodes, the gain coefficient is proportional to the current I through the diode. By taking the losses and also the reflectivities R_1 and R_2 of the mirrors of the cavity into account, we find

$$P \propto \alpha_g(I)l_g - R_1 R_2 \alpha_\ell d \propto I - I_{\text{th}}, \quad (2.16)$$

where we summarized the total losses in a constant I_{th} , the threshold current. Because the output power represents the power transferred by the photons emitted by the laser, we can relate the output power to electron-hole recombinations. By dividing the current through the elementary charge e , we get the number of electron-recombination processes per unit time. Multiplying this result by the photon energy $\hbar\omega_{\text{cv}}$, we obtain

$$P \propto \frac{I - I_{\text{th}}}{e} \hbar\omega_{\text{cv}}, \quad (2.17)$$

where $\hbar\omega_{\text{cv}}$ is the energy between the electron in the conduction band and the hole in the valence band. Now we have to consider that not every electron contributing to the current will lead to an electron-hole recombination. Some of the electrons can flow into different energy bands or excite phonons rather than creating a photon. For this reason, we introduce an efficiency constant $\eta < 1$ that gives us the final result

$$P(I) = \eta \frac{\hbar\omega_{\text{cv}}}{e} (I - I_{\text{th}}). \quad (2.18)$$

This result shows that the laser diode starts lasing if a minimum threshold current I_{th} is applied. The threshold current depends on the losses in the cavity as well as the reflectivity and is a constant in I .

Let us now compare this theoretical function describing the output power with the experimental data that I measured for the laser I built. The output power P was measured with a power meter while the current was modulated linearly from $I_{\text{init}} = (38 \pm 0.5)$ mA to $I_{\text{final}}(138.7 \pm 0.5)$ mA. The modulation frequency was 50 mHz, because for frequencies higher than 0.5 Hz a low-pass filter damped the modulation and to avoid this, the current was scanned slowly. In Fig. 2.7 the measured results with a linear fit function according to Eqn. (2.18) are shown. At about 87 mA a strong increase in output power can be seen. Below this current the emitted light is dominated by spontaneous emission. The threshold current could be determined to $I_{\text{th}} = (85.5 \pm 0.6)$ mA. One part of the error is from the error in I_{init} and I_{final} . Moreover, errors occur from the different starting points of the fitting function because just the part of the data curve

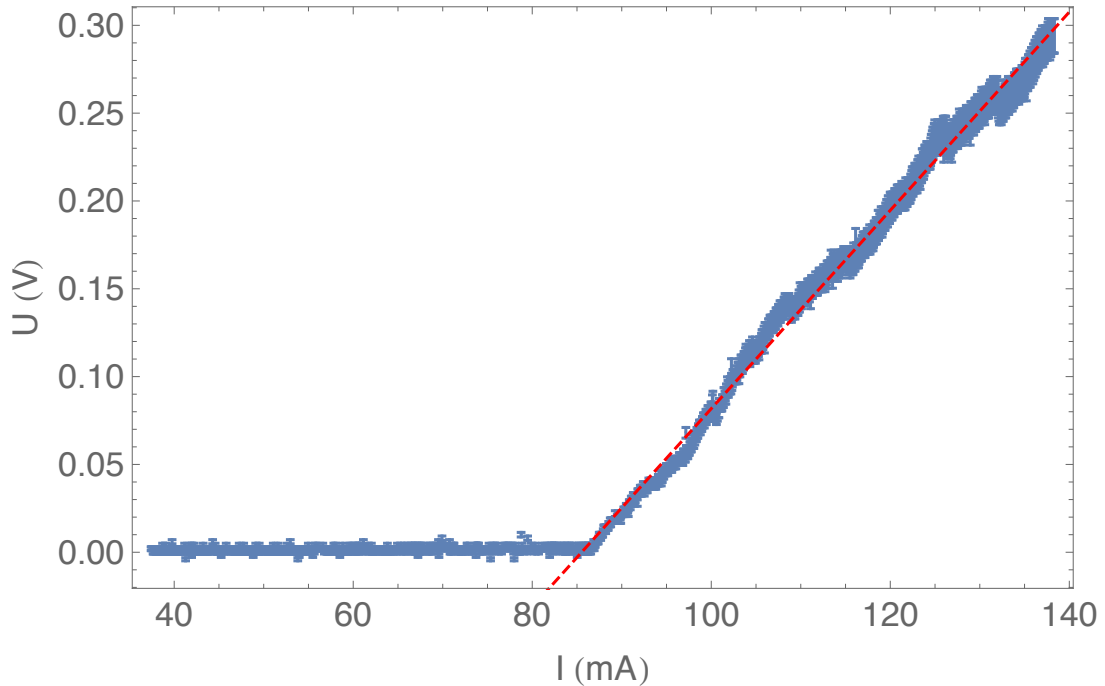


Figure 2.7: The current was modulated by a function generator with a saw tooth output voltage. The horizontal axis in this plot has been converted to a current through the laser diode. The vertical axis shows the output voltage of the power meter. A linear function is fitted and we obtain a threshold current of $I_{\text{th}} = (85.5 \pm 0.6)$ mA.

with a high slope should be fitted. Since the cut-off current had an influence on the fitted function, several fittings with different cut-off currents were done and then averaged. Additionally some minor errors appear because of fluctuations of the scope in the order of ± 1 mV and the accuracy of the power meter is given by $\pm 3\%$ which is why the error bars give the impression of a diverging curve in Fig. 2.7 for higher currents. To avoid the error due to the different fits, the behavior of the output power below threshold should be taken into account to have a model for the complete measured data. As you can also see in the plot, the output power above threshold is not perfectly a linear function. This might be due to mode-hops which we will discuss later in Ch. 5.1.2. These mode-hops could indeed be observed on the wavemeter while doing the measurement.

2.5 Gratings

To understand how an external cavity diode laser works, we have to discuss gratings and especially blazed gratings. Diffraction gratings are optical elements with

equidistant grooves that are either reflective or transmissive. We will first consider transmissive gratings and then apply our discussion to reflection gratings. The sign convention for the angles we use follows the convention shown in Fig. 2.8.

If light hits the surface of a grating, it is not only transmitted but also diffracted

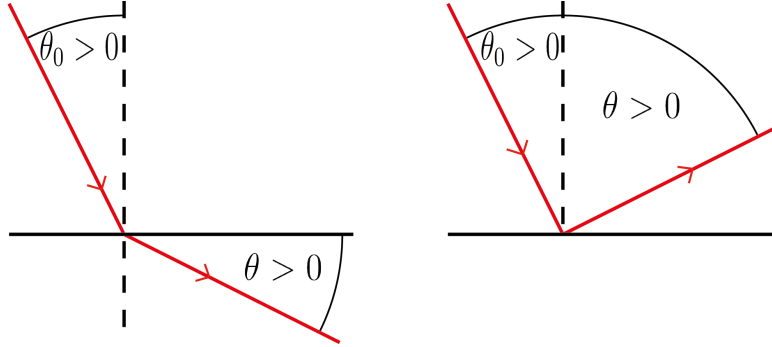


Figure 2.8: Convention of the sign of angles.

with different intensity in different directions. The grating equation

$$n\lambda = d(\sin \theta - \sin \theta_0) \quad (\text{grating equation}) \quad (2.19)$$

gives us the location of local maxima of the intensity distribution, where n is the order of diffraction, λ is the wavelength and θ_0 (θ) is the angle of the incoming (outgoing) beam related to the grating's normal. In the next chapter we would like to consider how Eqn. (2.19) can be derived by the Fraunhofer approximation.

2.5.1 Grating in the Fraunhofer Approximation

Let us remember Fraunhofer diffraction [16] which describes the intensity pattern of a plane wave being diffracted by an object in the far-field approximation. This approximation requires the Fresnel number $N_F = \frac{a^2}{\lambda d}$ to be small, i.e. $N_F \ll 1$, where a is the dimension of the object, λ the wavelength and d the distance between the object and plane of observation. We define the coordinates in the plane of our object with $\mathbf{X} := (\xi, \eta)^T$ and write the transmission function of the object as $\Omega(\xi, \eta)$ (see Fig. 2.9). The idea behind Fraunhofer diffraction comes from Huygens principle. The principle assumes that every point of the object Ω is the source of a spherical wave if the object is illuminated. Those spherical waves interfere and the Fraunhofer diffraction describes the interference at far distances from the object plane. The intensity pattern is then approximated by

$$I(\mathbf{k}_\perp) \propto \left| \int_{-\infty}^{+\infty} \Omega(\xi, \eta) \exp[-i(\mathbf{k}_\perp - \mathbf{k}_{\perp,0})\mathbf{X}] d\mathbf{X} \right|^2 \propto |\mathcal{F}[\Omega(\mathbf{X})]|^2, \quad (2.20)$$

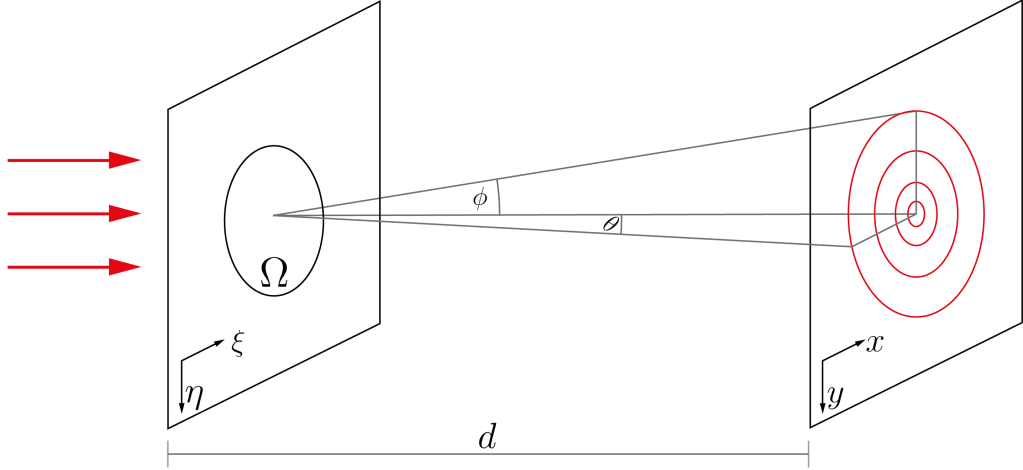


Figure 2.9: Ω is the diffracting object. The intensity pattern is observed on a plane at distance d . The angle θ (ϕ) gives the diffraction in the x (y)-direction.

where $\mathbf{k}_\perp := (k_x, k_y)^T$ and $k_i = \frac{2\pi}{\lambda_i}$ ($i = x, y$) are the wavenumbers in the i -direction of the outgoing beam and $\mathbf{k}_{\perp,0} := (k_{x,0}, k_{y,0})^T$ is the wavenumber of the incoming beam. Thus, the intensity pattern in the Fraunhofer approximation is proportional to the absolute value of the Fourier transform \mathcal{F} of the object function $\Omega(\xi, \eta)$. This is a useful result because we can easily calculate the effect of a plane wave illuminating an arbitrary object. Moreover, what is of interest to us, is the angular distribution of the intensity pattern. From Fig. 2.9, you can geometrically see that

$$\sin \theta = \frac{k_x}{\sqrt{k_x^2 + k_y^2 + k_z^2}} = \frac{2\pi k_x}{\lambda} \Leftrightarrow k_x = \frac{\lambda}{2\pi} \sin \theta \quad (2.21a)$$

$$\sin \phi = \frac{k_y}{\sqrt{k_x^2 + k_y^2 + k_z^2}} = \frac{2\pi k_y}{\lambda} \Leftrightarrow k_y = \frac{\lambda}{2\pi} \sin \phi. \quad (2.21b)$$

Further, we would like to calculate the effect of a grating on a plane wave in the Fraunhofer approximation by applying Eqn. (2.20). The function $\Omega(\xi, \eta)$ is in this case a sum of N equidistant grooves of the same form

$$\Omega_{\text{grating}}(\xi, \eta) = \sum_{m=0}^{N-1} \Omega_{\text{groove}}(\xi - ma), \quad (2.22a)$$

$$\Omega_{\text{groove}}(\xi) = \begin{cases} 1 & -\frac{b}{2} < \xi < \frac{b}{2} \\ 0 & \text{else,} \end{cases} \quad (2.22b)$$

where Ω_{groove} is the object function of a single groove of width b , and a is the distance between the grooves. Because the grating is approximated as infinitely large in the η direction, the function does not depend on η .

Now, we could just calculate $\mathcal{F}[\Omega_{\text{grating}}]$ in a straightforward manner, but there is a more elegant and simpler approach, since Ω_{grating} is a periodic function in Ω_{groove} . Hence, we can get this periodic function by convolution of the groove-function with a comb of N δ -distributions spaced by a :

$$\Omega_{\text{grating}}(\xi) = \left[\sum_{m=0}^{N-1} \delta(\xi - ma) \right] * \Omega_{\text{groove}}(\xi) \quad (2.23)$$

Now we apply the convolution theorem $\mathcal{F}[f * g] = \mathcal{F}[f] \cdot \mathcal{F}[g]$ from which it follows that

$$\mathcal{F}[\Omega_{\text{grating}}(\xi)] = \mathcal{F} \left[\sum_{m=0}^{N-1} \delta(\xi - ma) \right] \cdot \mathcal{F}[\Omega_{\text{groove}}(\xi)], \quad (2.24)$$

i.e. we can separate the calculation into two Fourier transforms and simply multiply the results afterwards. The derivation of both integrals can be found in Appendix A. We find with $x := \sin \theta - \sin \theta_0$:

$$I_{\text{groove}}(x) = I_{\text{groove}}(0) \left[\frac{\sin \left(\frac{\pi bx}{\lambda} \right)}{\frac{\pi bx}{\lambda}} \right]^2 = I_{\text{groove}}(0) \text{sinc}^2 \left(\frac{\pi bx}{\lambda} \right) \quad (2.25a)$$

$$I_{\text{comb}}(x) = I_{\text{comb}}(0) \left[\frac{\sin \left(N \frac{\pi}{\lambda} ax \right)}{N \sin \left(\frac{\pi}{\lambda} ax \right)} \right]^2 \quad (2.25b)$$

$$I_{\text{grating}}(x) = I_{\text{comb}}(x) I_{\text{groove}}(x) \quad (2.25c)$$

From Eqn. (2.25b) the grating equation (2.19) could be reproduced by finding the maximum values. In case of a grating the number N of illuminated grooves is usually a few hundred to a few thousand so that the sine function in the denominator of Eqn. (2.25b) oscillates much faster than the modulation of the sinc function in Eqn. (2.25a). Therefore the comb-pattern determines the structure of the intensity distribution with its local maxima while the effect of the finite groove size is the envelope of the intensity pattern.

2.5.2 Blazed Gratings

At last, we discuss a blazed grating. The grooves are now not transmissive but in the ideal case areas of reflectivity 1. Again Huygens principle holds but we have

to consider reflected waves from which we can calculate the intensity pattern in the Fraunhofer approximation. If we neglect the interference of the incoming and outgoing waves we can again make use of Eqn. (2.20). The grooves of a blazed grating are not parallel to the grating's surface but have a certain angle as you can see in Fig. 2.10. By using this shape, we can vary the amount of intensity between the different orders of diffraction. Therefore we have to change the

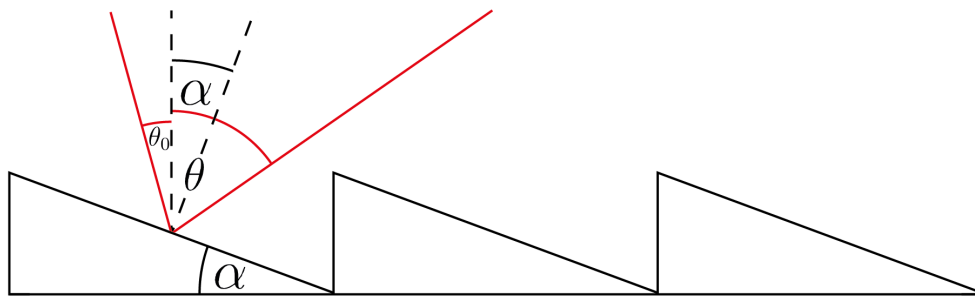


Figure 2.10: Schematic drawing of a blazed grating, where the grooves include an angle α to the grating's normal. In our convention the angles in the figures are counted positive.

groove function Eqn. (2.25a) and afterwards multiply it with I_{comb} again. The modification we have to do with I_{groove} is to shift the angle of zero order by 2α , where α is the blaze angle,

$$I_{\text{groove}}(\theta) \rightarrow I_{\text{groove}}(\theta + 2\alpha). \quad (2.26)$$

The zeroth order of diffraction is the geometrical reflected beam and this angle changes if the surface of grating is rotated. The intensity pattern with and without blaze angle is plotted in Fig. 2.11. The top row shows a grating with just $N = 8$ slits illuminated and an angle of incidence (AOI) of 0° . The bottom row is a simulation of the grating I used for my laser with $\text{AOI} = 43.55^\circ$. The left panel in the bottom row shows the result without blaze angle and the right panel uses a blaze angle of $\alpha = 28.36^\circ$. The intensity in the first order of diffraction dramatically increases when using a blazed angle, as can be seen as a shift of the envelope function to the right hand side of the plots.

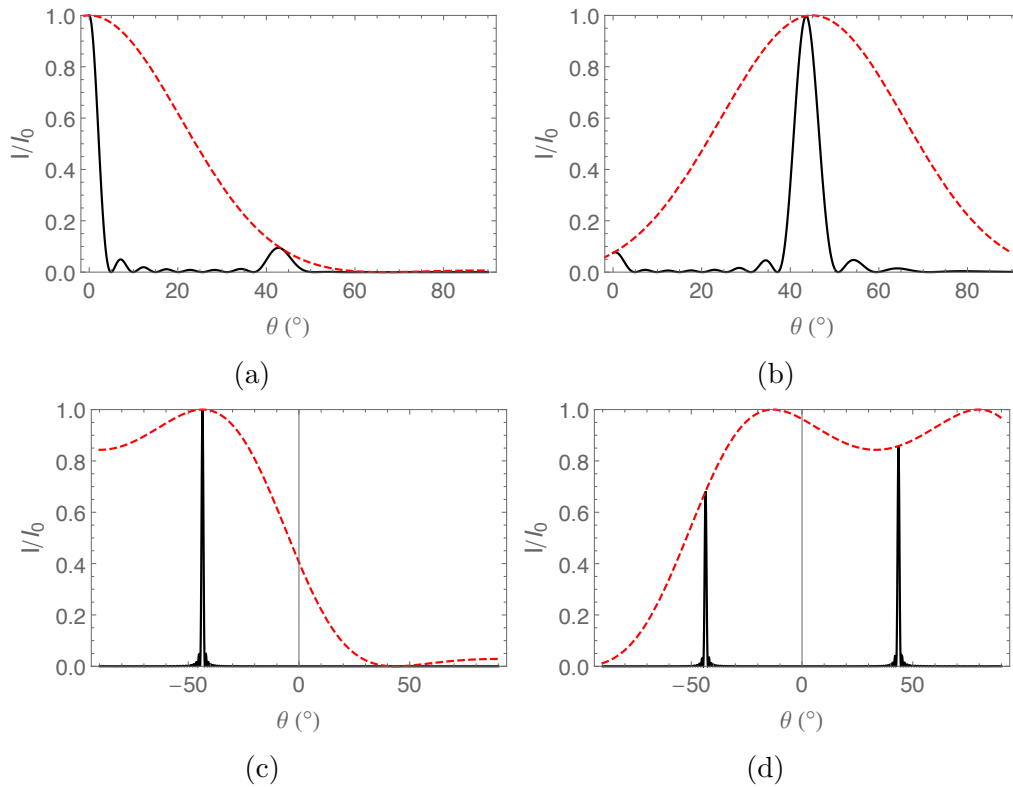


Figure 2.11: The figure shows the effect of a blaze angle on the intensity pattern. For all plots $\lambda = 689 \text{ nm}$. The black line is the intensity distribution, while the dashed red line shows the envelope caused by the finite size of the single groove. Top row: A grating with 1000 grooves/mm = $1/a$, groove size $b = 0.75a$, with $N = 8$ grooves illuminated and $\text{AOI} = 0^\circ$ is simulated. Bottom row: The grating I use with 2000 grooves/mm, groove size $a = b$, $N = 100$ grooves illuminated and $\text{AOI} = 43.55^\circ$ is simulated. Panel (a) and (c) show a non-blazed grating, while panel (b) shows a grating with blaze angle $\alpha = 22.5^\circ$ and panel (c) has $\alpha = 28.36^\circ$.

2.6 Laser Designs

There are several designs to implement a tunable laser. In this chapter two tunable lasers, the Littrow and the Littman laser, are presented and later compared. In both designs a laser diode is used and the relevant laser cavity is formed externally instead of the internal diode cavity. For this reason, these designs are classified as External Cavity Diode Lasers (ECDL).

2.6.1 Littrow Configuration

The laser design considered in the following is a so-called Littrow laser [17, 18]. There, the cavity resonator consists of one fixed mirror and a reflection grating with a gain medium in between (see Fig. 2.12). The grating has two functions:

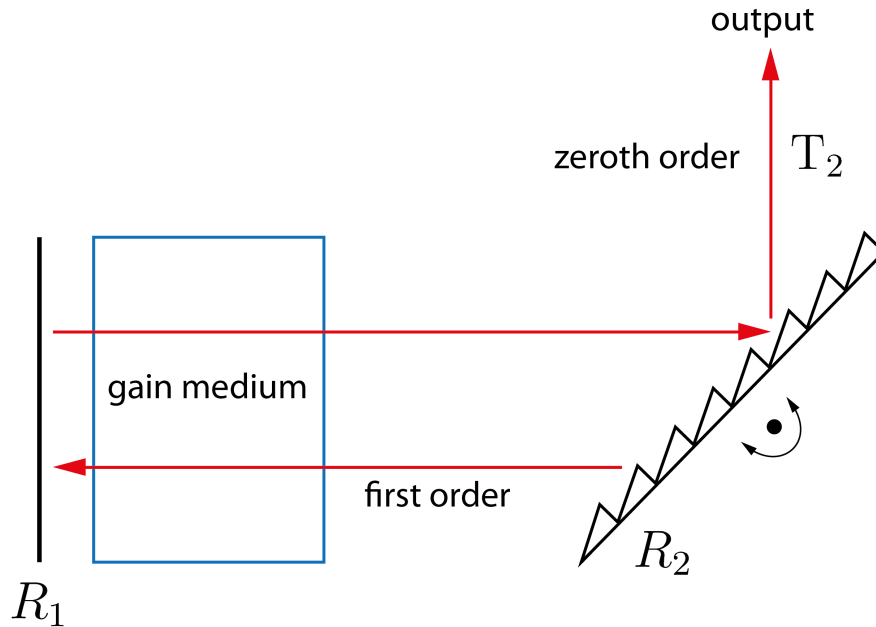


Figure 2.12: The Littrow configuration consists of a fixed mirror, here on the left side of the figure, with reflectivity R_1 , a grating, here on the right side, that can be rotated, and a gain medium. The first order of diffraction travels back to the gain medium and this reflection coefficient is indicated with R_2 . The transmission of radiation reflected into the zeroth order of diffraction is called T_2 here.

First, it has to work as a back-reflector to create laser oscillations and form a resonator with the fixed mirror. Second, the grating must work as a mirror that couples some of the light out of the resonator. Both of these functions can be done by a grating. In general, the grating equation (2.19) has to be fulfilled. If the incoming and outgoing beam of first order of diffraction are congruent, i.e. $\theta = -\theta_0$, then the arrangement is called the Littrow configuration. In this case Eqn. (2.19) simplifies to $\sin \theta = \frac{\lambda}{2d}$ for $n = 1$. The condition $n = 1$ means that we want to have no other order of diffraction in between the back-reflected beam and the out-coupled beam, which has order $n = 0$. By rotating the grating, the wavelength reflected back into the laser medium (and thus the wavelength at which the laser runs) can be selected. The tunability is limited by the wavelengths at which the gain medium can be stimulated. We can control the reflectivity by the blaze angle of our grating, which is important to the performance of our laser as we know from Ch. 2.3.

2.6.2 Littman Configuration

In addition to the Littrow configuration, there is the similar Littman configuration [17]. Here, the beam coming from the gain medium hits a fixed grating and the zeroth order of diffraction is coupled out. The first order of diffraction propagates to an additional mirror that can be rotated. The beam coming from the mirror is then reflected back to the gain medium by the grating as shown in Fig. 2.13. By rotating the mirror, the wavelength coupled back to the laser medium can be chosen and again the laser is tunable as in the Littrow configuration.

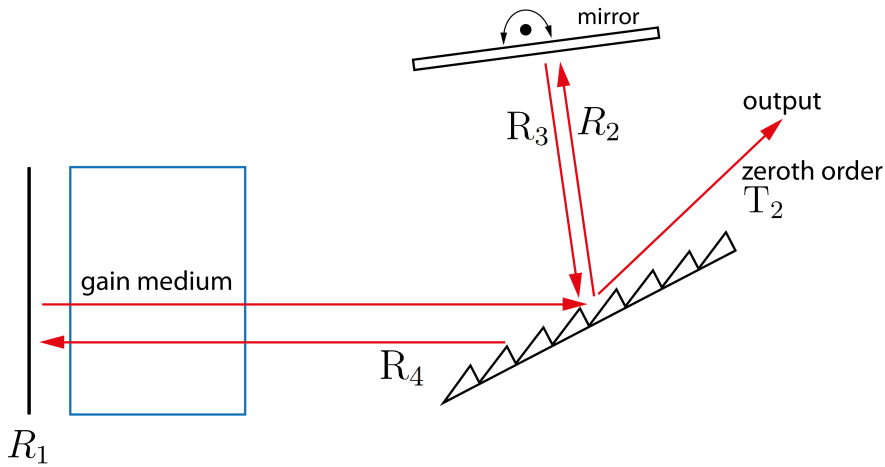


Figure 2.13: The Littman configuration has a fixed mirror, here on the left side of the figure, a grating that is fixed, and a gain medium in between. Additionally there is a rotatable mirror that provides tunability by choosing the wavelength reflected back to the gain medium. In contrast to the Littrow configuration, more reflection coefficients have to be considered.

2.6.3 Littrow vs. Littman Laser

Both the Littrow as well as the Littman laser are tunable in wavelength by the frequency selective grating. One advantage of the Littman configuration is a fixed direction of the outgoing beam. Even if the wavelength is tuned, none of the optical components after the laser have to be adjusted, while in Littrow configuration, the grating itself is rotated and thus the direction of the beam changes. Moreover, the Littman laser is more stable towards mode-hops than the Littrow laser because the wavelength selection happens two times on the grating. Therefore the beam reflected back into the gain medium is more narrow in bandwidth.

In contrast to the Littman laser, the Littrow laser provides a higher output power. Because this was more important to us, a Littrow laser was built.

Chapter 3

Design and Setup

In this chapter I would like to present the design of the laser and report on the setup. The description of the setup points out problems that came up during the assembling and suggests possible solutions. In the end, I will discuss methods for minimizing the threshold current to obtain maximum output power as well as the optimization of the temperature controller which is required for the long-term stability of the laser.

3.1 Mechanical Design

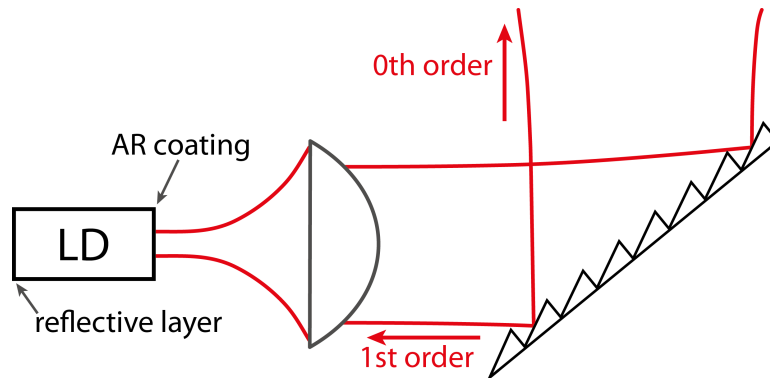


Figure 3.1: The left side of the laser diode has a reflective layer while the layer on the right side has an anti-reflection coating. The diverging beam is collimated by a lens.

The description of a Littrow Laser in Ch. 2.6.1 is very schematic. To implement this design a semiconductor diode laser (LD) is used. Usually a LD itself forms a cavity by two reflective planes. Because we want to have the grating as one

of the mirrors of our cavity, the LD has an anti-reflection (AR) coating on the side pointing towards the grating. Moreover, the small size of the gain medium leads to a great divergence angle. That is why a collimation lens is put between the LD and grating to have an approximate plane wave hitting the grating and correspondingly sharp orders of diffraction. This configuration can be seen in Fig. 3.1.

The mechanical design I used for my 689 nm Littrow laser was made and optimized by the Steck Lab at the University of Oregon [1]. It promises a linewidth in the kHz range. The design was modified by A. Mayer at MPQ for compatibility with metric units. A manual with pictures of the assembly by the Steck Lab is available online in Ref. [19].

The case is machined from an aluminum block and consists of a base-plate, the main case with the grating arm and the bottom and top plate of the cavity as you can see in Fig. 3.2. Between the grating arm and a fine adjustment screw sits

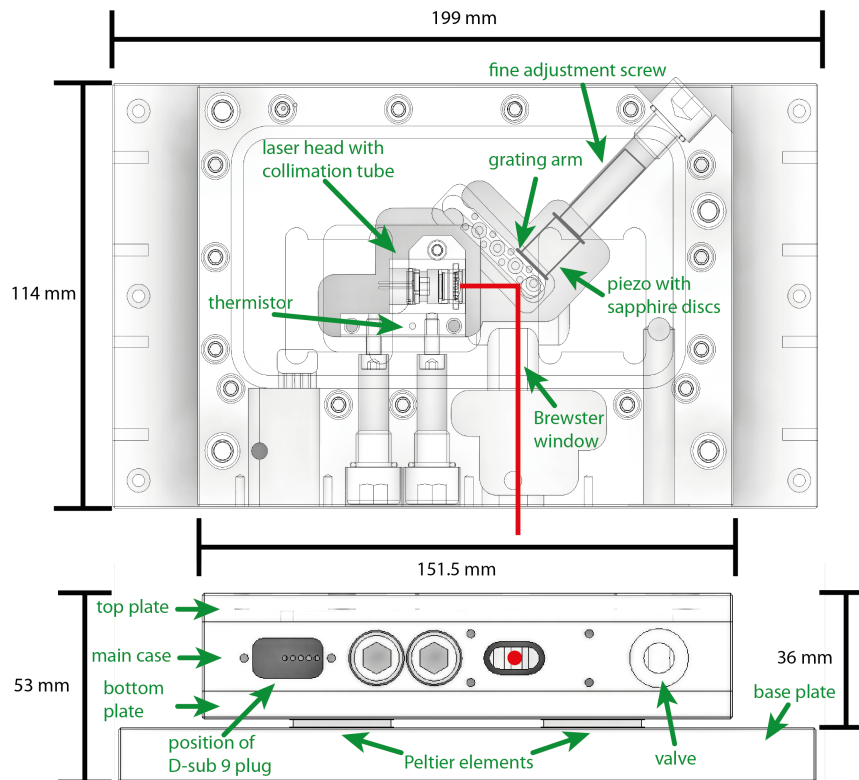


Figure 3.2: Drawing of the ECDL design with the position of the important features.

a piezo-stack with sapphire-glass discs glued onto each end by *Torr Seal*. The fine-adjustment screw can bend the grating arm for approximate fixing of the correct position. By applying voltage to the piezo we can then fine-tune the grat-

ing to the desired angle. The grating arm is machined at an initial angle of 47° with respect to the laser beam and is designed to be used at a 45° angle. In this position, the grating arm is still flexible enough to rotate in both directions and we can thus scan the laser's wavelength. Below the grating arm sits an additional O-Ring to damp mechanical vibrations especially at ~ 14 kHz as described in Ref. [1].

To provide temperature control, a thermistor sits in a hole in the laser head to measure the temperature next to the laser diode. For heating and cooling two Peltier elements are positioned between the base-plate and the bottom plate of the cavity.

3.2 Sonication

To protect the optical elements and the laser diode from dust and other impurities as well as to potentially place the cavity in a vacuum, all parts were cleaned before assembly. The cleaning process removes dirt, machine oil and other undesired substances. Thus, the aluminum parts and Kapton wires were put into a bath with distilled water and soap. The screws as well as the collimation tube, O-Rings and sapphire disks were put together with isopropanol into a beaker. Then the bath was treated by a procedure called "sonication" at 40°C for 10 min. In the ultrasonic bath waves with a frequency of 38 kHz are produced in the water and isopropanol by the Sonicator (*Sonoswiss SW 90 H*). The ultrasonic waves in the water create bubbles that first grow and then collapse. This leads to localized, high temperatures of about 5000 K and thus to a thermal dissociation of water that recombines to reactive radicals. These radicals can dissolve organic compounds on the surface of the materials and thus clean them [20].

After sonication every surface was rinsed per about 10 seconds with deionized water except for the screws and collimation tube. Then the parts were again flushed by acetone and isopropanol. In a final step I again rinsed every part with deionized water to remove the chemicals and dried the parts on aluminum foil over night. The collimation tube and the screws were not treated with water because it dries slowly from the thread at room temperature while acetone has a boiling point at 56°C ¹ and evaporates therefore faster. Moreover, no acetone was applied to the O-Rings to protect the material which is chemically soluble in acetone. After this sonication procedure, the cleaned parts were touched only with cleanroom-grade nitrile gloves.

¹<https://en.wikipedia.org/wiki/Acetone>

3.3 Brewster Window

The outgoing laser beam leaves the cavity through a plate of glass. This window is used to isolate the cavity from influences of the environment, e.g. temperature fluctuations or diffusion of air. It is glued onto the mount with the two-component vacuum-tight glue *Torr Seal* and dried at room temperature.

Because the laser beam crosses different media (air/vacuum - glass - air), reflections occur that we want to minimize to get maximum output power. Thus, the window is positioned at Brewster's angle θ_B to prevent reflections of s-polarized light. Here s-polarized light is defined as perpendicular to the plane of the optical table and therefore parallel to the plane of incidence on the window. We position the LD by rotating the collimation tube to obtain s-polarized emitted light. Brewster's law describes the angle for which the reflection of s-polarized light from the window vanishes.

Brewster's angle [16] is given by $\theta_B = \arctan\left(\frac{n_{\text{glass}}}{n_{\text{air}}}\right)$ and with $n_{\text{air}} \simeq 1$, $\theta_B = 57^\circ$ which is pre-machined into the aluminum case. It follows $n_{\text{glass}} = \tan(\theta_B) = \tan(57^\circ) = 1.540$. The glass I used was cut by a glass cutter from a microscope slide. If we assume that it is made out of made of borosilicate glass BK7, it has a refractive index of $n(689 \text{ nm}) = 1.513$ that can be calculated by Sellmeier's formula [21]. Therefore the reflection should not be zero but is still strongly suppressed by this angle of the window with respect to the beam.

3.4 Temperature Control Elements

For running the laser on the same mode and at constant output power, we have to accomplish stable external conditions and have to control the laser's temperature. A change in temperature leads to thermal expansion of both the external cavity and the LD. Furthermore the refractive index of the semiconductor material also depends on temperature [22]. Hence, the properties of the laser resonator are influenced by the temperature controller which should on one hand be able to hold a constant temperature for stable performance of the laser and on the other hand should be able to adjust the temperature in a defined way to optimize the laser. In this section the mounting of the temperature control elements is described and later in Ch. 3.9.2 the electronic controller is discussed.

For temperature measurement a 10 k Ω NTC (Negative Temperature Coefficient) thermistor (EPCOS, RS 528-8536) is used and later connected to an external *Toptica* controller. It uses the dependence of electrical resistance on temperature and computes the temperature by Ohm's law $R = U/I$ with voltage U and current I . The thermistor sits next to the laser diode at an approximate distance of 10.4 mm and is fixed inside a hole in the aluminum laser head by glue (EPO-TEC[®] H77). This two-component glue is thermally conductive and electrically insulating with a recommended mass mixing ratio of Part A and B of 100 : 15.

For curing, the laser head with thermistor was baked at 150 °C for 210 min. To control the temperature, two Peltier modules (ETH-071-14-15, RS 490-1480, $I_{max} = 6$ A) are soldered in series and placed between the base-plate and bottom plate. A Peltier element or TEC (Thermoelectric cooler) makes use of the Peltier effect. The Peltier effect describes the heat transfer at an interface of different conducting materials while current flows. This effect is much greater if one of the material is a p-/n-doped semiconductor. The direction of current determines if the junction gets cooled or heated. The advantage of Peltier elements is that both heating and cooling can be done by the same component. For further reading on the Peltier effect (and the reverse Seebeck effect) Ref. [14] is recommended. The orientation of the modules is important. In my case the hot side is the one where the wires are connected, as you can see in Fig. 3.3. To support thermal conductivity both sides of the Peltier elements are greased with a thin layer of thermal paste (WLPF from *Fischer Elektronik*).

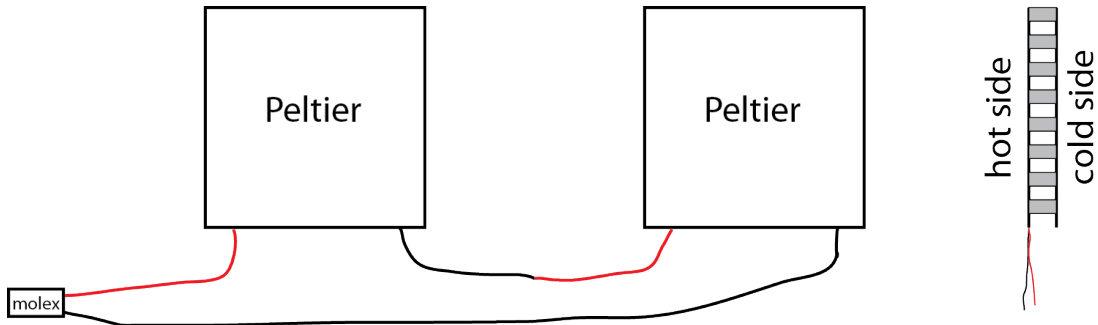


Figure 3.3: Sketch of the Peltier elements I used from top and side view with orientation of the hot and cold side. The red (black) wire indicates the anode (cathode).

3.5 Electronic Circuit

The electronic elements, i.e. Peltier modules, thermistor, piezo and laser diode, are controlled by a *Toptica* console and the electronics are connected by a D-Sub 9 plug. To both protect the laser diode and also to provide current modulation ports, an additional protection board is used.

3.5.1 D-Sub 9 Connection

The wires that are used inside of the aluminum case have to be vacuum compatible. Thus, wires with a Kapton insulation are chosen and soldered to the electronics. Because the insulation of the piezo connecting wires and of the thermistor are made from Teflon, these wires were shortened. The Kapton wires enter

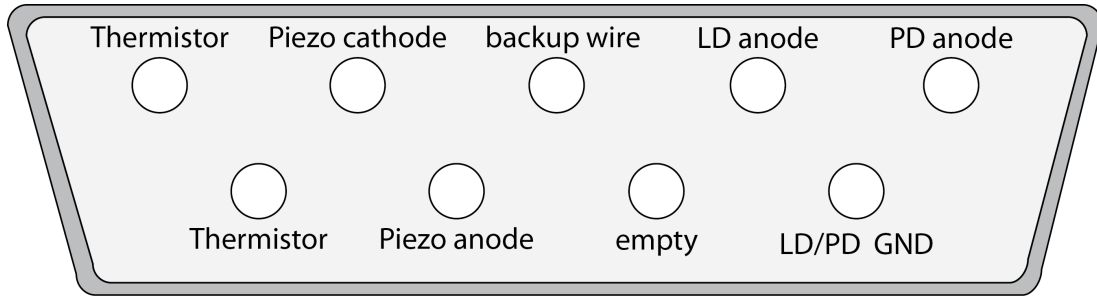


Figure 3.4: Front view of the D-Sub 9 female plug and order of the pins.

the main case through five holes that can be seen at the position of the D-Sub 9 plug in Fig 3.2. Especially the connections to the laser diode do not share the holes with other wires to reduce disturbance by magnetic fields of the different currents, e.g. from large modulation of the piezo. To vacuum seal the holes and to fix the wires into the case, the two component glue *Loctite 1C Hysol* was used and cured at room temperature. This glue was chosen because it is less viscous than *Torr Seal* and hence it fills the bores more easily.

Later we would like to plug or unplug the laser without opening the case or soldering any connection, so a D-Sub 9 female plug is mounted from outside to the case. My choice of ordering the pin contacts can be seen in Fig. 3.4. It is recommended to document the pin connections properly during soldering to be sure that the laser diode has the correct connectivity. Because I decided to install the wires of the Peltier elements outside of the case, I did not connect them to the D-Sub 9 plug but instead I used a *Molex KK* plug for the Peltiers. That is why two pins of the D-Sub 9 are not in use and I soldered one more Kapton wire to it which also runs into the main case, so that if another wire breaks, there is a backup wire.

3.5.2 Protection Board

As mentioned above an additional protection board is integrated between the D-Sub 9 plug of the laser itself and the *Toptica* controller. The whole circuit is attached in the appendix B. The board offers the following features:

- A combination of four low-pass filters protect the laser diode from voltage spikes in the power supply.
- Schottky diodes protect the laser diode if the wrong input voltage polarity is applied.
- A relay shunts the laser diode as soon as it becomes disconnected from the power supply to protect it from electrostatic discharges.

- The current can be scanned by a DC modulation part using a SMA plug.
- Some space on the board is left empty for an AC modulation part that can be soldered later if required.
- The power supply is decoupled from the modulation modules.
- Test points for a four-point measurement to determine the current running through the LD. The foil resistor used here has a resistance of $R = 0.1 \Omega$ and by measuring the voltage, the current can be calculated by $I = U/R = (10U) \Omega^{-1}$.
- If a photodiode is integrated in the case of the laser diode, the signal can be amplified and can be read out from a SMA connector. The photodiode amplifier requires an external $\pm 15V$ power supply.

Be aware that a JFET in the DC modulation circuit steals about 9 mA that has to be subtracted from the value of the current on the *Toptica* console. A more detailed description of the protection board can be read in the master's thesis of Nejc Janša [23].

3.6 The Laser Diode and Collimation Tube

The laser diode has a front facet antireflective (AR) coating with an intensity reflectivity of $3 \cdot 10^{-4}$. It has a center wavelength of about 685 nm and is produced by *Eagleyard Photonics* (EYP-RWE-0690-00703-1000-SOT02-0000). The recommended operational parameters are a maximum current of $I_{max} = 140$ mA and a temperature between $15 - 20^\circ$ C.

The diode is connected to a 3-Pin socket that is soldered to the Kapton wires mentioned in Ch. 3.5.1. The pin assignment of my diode can be seen in Fig. 3.5. The polarization of the emitting radiation is in the plane of the LD anode and PD anode pin. Be aware that the assignment and direction of polarization varies between diode models.

There was a problem coming up when plugging the pins into the socket because the sockets available in our lab have the wrong pin diameter and could not be mounted to the diode. We now use another socket that is not ideal because the designated pin circle diameter is too small. The pin circle diameter determines the distance between the pins themselves and, unfortunately, with this socket the pins get deformed. Next time this diode is mounted, new sockets might have to be used. The diode's manufacturer recommends a certain socket (R100-0403-04N-75S-R15-L14 by *Andon electronics*) that was also tried out but did not work because the socket holes were too wide to hold the diode pins safely.

To position and to align the laser diode, it is mounted in a collimation tube

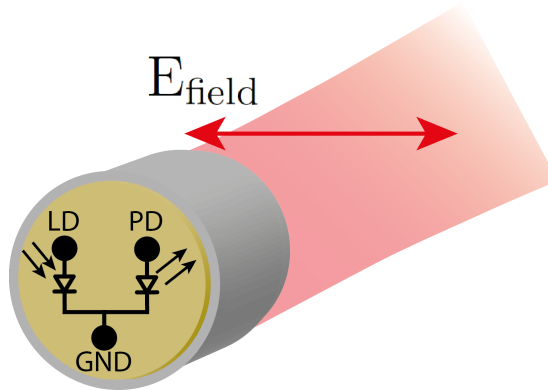
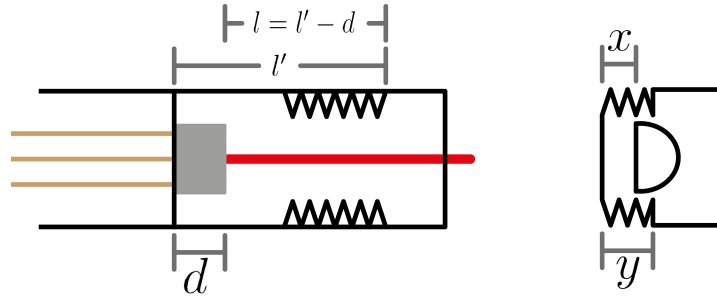


Figure 3.5: Sketch of the back view of my laser diode with the pin connection indicated. The LD and PD pins are connected to the anode and the GND pin to the ground. The polarization of the emitted light is parallel to the anode pins.

(*Thorlabs LT110P-B*) with an AR coated aspherical lens (*Thorlabs C610TME-B*, $f = 4.00$ mm, $WD = 2.44$ mm, $NA = 0.60$). In my case, the laser diode does not have the correct dimension for the collimation tube design from *Thorlabs* and new lenses had to be bought. When planing a new Littrow laser, you should consider the following:

The case of the diode has a plane at which it is mounted in the collimation tube. Relative to this plane the light emitting area is located in a distance d (for my diode $d = 3.65$ mm). Because the dimension of the light emitting area in a semiconductor diode is usually in order of a few μm , it can be assumed as a point source. Thus, this point source should sit in the focus of the collimation lens. The *Thorlabs* collimation tubes are designed to mount diodes with $d = 1.7 - 3.2$ mm and this limit comes from the finite axial extend of the threads. If d is out of this range, the correct choice of the collimation tube and lens has to be made. You also have to keep in mind that the focus of a lens is not just at the distance of the focal length to the lens' surface but is given by the working distance WD. Figure 3.6 shows the size of the different collimation tubes offered by *Thorlabs* and their dimensions. So if you decided on a certain tube, you should calculate $l = l' - d$, where l' is the distance between the mounting plane and the begin of the thread from the tubes aperture. Then $WD < (l + x)$ has to hold with x as the distance between the lens surface and end of its thread. Because the thread of the lens has finite size y the WD has also a lower bound and therefore $l - y + x < WD < l + x$. The WD should be somewhere in the middle of these boundaries.

When the correct lens and collimation tube are found, the diode can be mounted. The LD is a sensitive electronic device and can be destroyed by electrostatic discharge. While operating with the diode you should always take care that both



Product name	l' in mm
LT110P-B	6.38
LT220P-B	10.82
LT230P-B	6.81
LT240P-B	8.92

Figure 3.6: Sketch of the collimation tube and mounted lens. The saw tooth shape indicates the thread. For many *Thorlabs* mountings of aspherical lenses $y = 3.2$ mm. The table shows the parameter l' for different *Thorlabs* tubes.

yourself and every tool that touches the LD is grounded.

3.7 The Grating

In Ch. 2.5 we discussed gratings and blazed gratings. Now I present my choice of grating and how it was mounted.

From the grating equation (2.19) and with the desired Littrow angle of $\theta = 45^\circ$ related to the grating's normal, we get $d = \frac{\lambda}{2 \sin \theta} = \frac{689 \cdot 10^{-9} \text{ nm}}{2 \sin 45^\circ} = 4.87 \cdot 10^{-4} \text{ mm}$ or $\frac{1}{d} = 2053 \text{ mm}^{-1}$. Because gratings with 2000 grooves/mm are standard gratings available for purchase, such a grating was chosen (*richardsongratings*, -059H). Because we cannot buy gratings with exactly the desired number of grooves, the angle has to be adapted to $\theta = \arcsin\left(\frac{\lambda}{2d}\right) = 43.55^\circ$. So the grating arm has to be bent from its initial position of 47° by $\Delta\theta = 3.45^\circ$ which is out of the elastic area of the aluminum flexure and plastic deformation occurs. That is why it is recommended to use an additional shim on one side of the grating. With a shim the grating is not flat on the aluminum anymore but has already an angle $< 47^\circ$ to reduce mechanical stress on the grating arm. I measured a thickness of about 0.2 mm of the shim with glue that gives with the grating's length of 12 mm an angle of about 1° related to the grating arm. The grating arm therefore has to be bent by $\Delta\theta = 47^\circ - 1^\circ - 43.55^\circ = 2.45^\circ$.

From the datasheet, we know that the maximum efficiency of diffraction is in Littrow configuration for a wavelength of $\lambda = 475 \text{ nm}$. This grating is not a blazed grating but a holographic grating. For this type the grooves are not tilted

by a triangle shape but in sinusoidal pattern which leads to a smoothening of the orders of diffraction. The advantage is that the effect of a blazed angle is symmetrical for both positive and negative angle of incident. If we approximate the holographic grating as a blazed one we can obtain the blaze angle. Since the blaze angle is for this grating equal to the Littrow angle for $\lambda = 475$ nm, we get $\alpha = \theta(475 \text{ nm}) = \arcsin\left(\frac{\lambda}{2d}\right) = 28.36^\circ$. The intensity pattern of $\lambda = 689$ nm and $\theta_0 = 43.55^\circ$ is shown in the previous chapter in Fig. 2.11.

To mount the grating on the arm, it was glued with *Torr Seal*. A positioning jig produced by our machine shop was put on the grating arm. It has the correct dimensions, so if the grating is put on it, the laser beam will hit the grating in its center. First the shim was glued with a very thin layer of *Torr Seal* and placed on the desired position. After the glue dried, the grating was carefully put down on the jig. Pay attention that the grooved surface is parallel to the grating arm, otherwise the diode can eventually not get feedback from the grating. Afterwards one drop of *Torr Seal* is used to fix the grating and as soon as the glue is cured the jig can be removed. Later, when the laser was working some more drops of glue were added for stability.

3.8 Aligning to Feedback

With the electronics, laser diode, collimation tube and grating we can get the LD to start lasing. To reach the lasing condition we have to align the laser head and lens position such that the first order of diffraction is reflected back into the semiconductor laser diode and gives feedback. By now at the latest the maximum current should be set on the current controller. It is recommended to connect a multimeter to the test points of the protection board while doing the next steps. First the beam has to be collimated and for this purpose the laser head has to be taken out of the case. If current runs through the LD, it starts emitting light but with low intensity which is due to spontaneous emission. The lens position has to be adjusted such that this emitted light is collimated on a far object e.g. a wall on the opposite side of the lab. Then the laser head is put back into the case and fixed by two M4 screws for fixing and two grub screws to adjust the angle between the beam and the baseplate. Now both the fine-adjustment screw as well as the grub screws have to be scanned while applying not maximum but a high current to the LD. If the first order of diffraction is directly sent back to the LD, i.e. it gets feedback, the LD starts lasing immediately that can be seen by a dramatic increase in output power. Usually this procedure beginning with collimation to the wall has to be repeated a few times. The reason is that if the diode is not lasing the emitted light is very weak and not locally confined. Therefore the light is hard to see on a far object and it is not clear to determine the point of collimation.

3.9 Optimization

After the laser is set up, it has to be optimized. This chapter contains instructions to minimize the threshold current to get maximum output power and to adjust the electronic controller for optimal temperature control.

3.9.1 Minimizing Threshold Current

The threshold current was discussed in Ch. 2.4.2. We found that the output power Eqn. (2.18) of a semiconductor laser diode is given by $P(I) = \eta \frac{h\nu_{cv}}{e} (I - I_{th})$. The threshold current I_{th} is dependent on the losses in the cavity due to e.g. scattering but also on the reflection coefficients of the cavity's mirrors (or the grating). We can minimize the threshold current by changing the amount of feedback. The properties of the grating, i.e. blaze angle and coating, that influence the reflectivity are fixed. The only degrees of freedom to change the feedback are thus the lens position and polarization of the incident wave.

Let us first consider the position of the lens. The intensity pattern of a wave diffracted by a grating in Fraunhofer approximation of Ch. 2.5 just holds if the incoming beam is a plane wave. The beam coming out of the laser diode is not a plane wave but a gaussian beam that has curved wavefront. By aligning the laser diode to a far off object, we tried to make the wavefront as plane as possible to get sharp orders of diffraction. By changing the position of the lens just slightly, we can change the intensity of the beam that gives feedback into the laser diode. A recommended way to find the feedback from which the highest output power results, is to start with a lens position where the beam is focused between the laser diode and a wall. The next step is to mount the laser head into the cavity and find the position where the laser gets feedback and measure the threshold current with help of a power meter. The final step is to take the laser head out again and rotate the lens in the direction so that the focus is now further away and again find out the threshold current. These steps should be iterated until the lowest threshold current is found. Be aware to always rotate the lens in the same direction during this procedure because of hysteresis of the threads. Hysteresis means in this context that after rotating the lens one step forward and the same step backward, the lens is not at the initial position again.

The second degree of freedom is the polarization of the beam that can be changed by rotating the collimation tube in the laser head. The polarization dependence on the reflectivity efficiency arises from the coating or grating's material. The collimation tube can be rotated and for each step the threshold current be measured. In my case, the grating filters the polarization strongly. I could lower the threshold current by a certain choice of polarization by about 20 mA. In this case, the zeroth order beam was still s-polarized light and the p-polarized light was not reflected but absorbed by the grating. For this reason the total output power at the maximum current was even smaller than for an incident s-polarized

light. Not only absorption of p-polarized light at the grating can affect the output power but also undesired reflections on the Brewster window that occur for light that is polarized perpendicular to the plane of incidence.

The lowest threshold current I could reach was $I_{\text{th}} = (85 \pm 0.6)$ mA as shown in Fig. 2.7 in the previous chapter. This leads to a maximum output power of about 22.5 mW that is slightly below the value ≈ 23 mW that can be found in datasheet of the laser diode. The operational conditions and optics *Eagleyard Photonics* used, are not known but assumed to be optimal. Therefore the output power I measured might already be the best I could reach without changing e.g. the blaze angle or the lens.

3.9.2 PID-Controller

The temperature control elements, i.e. the thermistor and Peltier modules (Ch. 3.4) are connected via the protection board to the temperature control device *DTC 110* from *Toptica*. In the following we introduce the principle of such a controller and afterwards we present a method for finding the optimum settings on the basis of the data I measured for our laser design.

All controllers work with a feedback loop. The idea is to take input signals where one is the set value and the other is a measurement of the same quantity from the system. The set value is e.g. the desired temperature for our laser and the signal is the measured temperature. Those two signals are subtracted and the result is an error signal e . The controller then manipulates the error signal and gives an output u to the system that is for example the current applied to the Peltier elements. The system reacts to the output, returns a signal and the loop starts again. To optimize our system we have to understand the process of the error signal manipulation. A typical mechanism to implement a feedback loop is a PID controller which is an abbreviation for Proportional-Integral-Derivative controller. The output is composed of three terms:

$$\begin{aligned} u(t) &= k_{\text{P}}e(t) + k_{\text{I}} \int_0^t e(\tau)d\tau + k_{\text{D}} \frac{de(t)}{dt} \\ &= k_{\text{P}} \left[e(t) + \frac{1}{T_{\text{I}}} \int_0^t e(\tau)d\tau + \frac{1}{T_{\text{D}}} \frac{de(t)}{dt} \right] \end{aligned} \quad (3.1)$$

The first term is proportional to the error signal e with proportional gain k_{P} and gives a correction to the system dependent on the current error. The second term integrates $e(t)$ over time and is weighted with the integral gain k_{I} . By integration, it takes errors from the past into account and is therefore responsible for long-term stability of the system. The last term contributes to the output with the value of the derivative of the error function multiplied with the derivative gain k_{D} . Because it is proportional to the derivative, it can be seen as an interpolation of the error signal and thus predicts errors in the future of the system. The gain

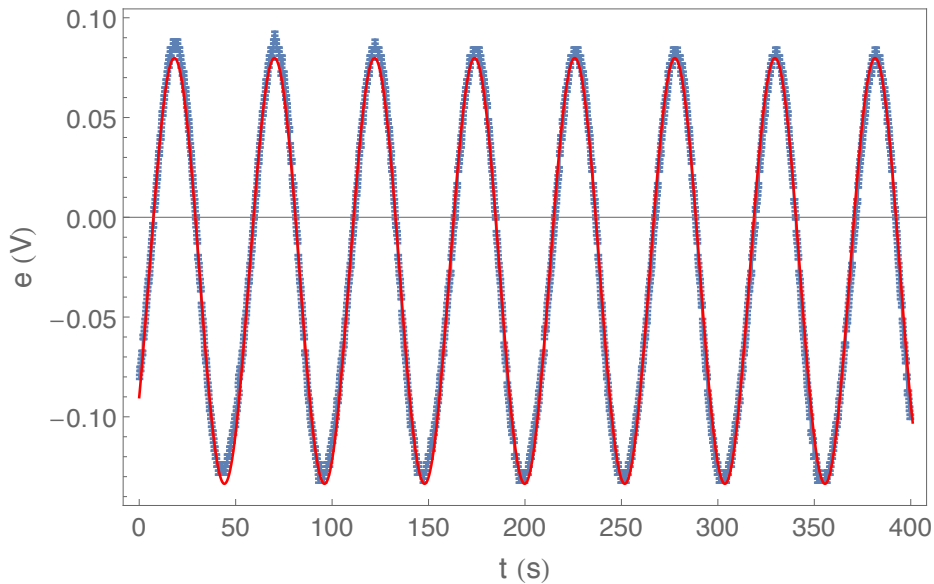


Figure 3.7: The error signal on the scope with $k_P = k_{\text{crit}}$ and $k_I = k_D = 0$. The blue dots show the measurement data with error bars and the red line is the fitted function. 1 V corresponds to 1 K on the temperature scale. The critical time is determined to be $T_{\text{crit}} = (51.89 \pm 0.01)s$.

factors k_P , k_I and k_D now have to be adapted to the specific system to be optimized in the sense of a fast decaying error signal and long-term stability. Parameters on which the factors are dependent are in the case of our temperature control system the efficiency of the Peltier elements, the thermal conductivity between the Peltier elements and the thermistor, and the thermal mass of the laser head. A procedure to find good parameters is the Ziegler-Nichols method [24]. In this procedure two characteristic values of the system have to be determined, the critical gain k_{crit} and the critical period T_{crit} . To this end we first set $k_I = k_D = 0$ and increase the proportional gain k_P until the system is oscillating around the set value with a constant amplitude. This value of k_P is then defined as k_{crit} and the time period as T_{crit} . If $k_P > k_{\text{crit}}$ the system is also oscillating but the amplitude is increasing. For $k_P < k_{\text{crit}}$ the error is a decaying oscillation that has a constant long-term drift. Once the critical parameters are found, the Ziegler-Nichols method predicts following optimum values for the gain parameters:

	k_P	T_I	T_D
P	$0.5k_{\text{crit}}$		
PI	$0.4k_{\text{crit}}$	$0.8T_{\text{crit}}$	
PID	$0.6k_{\text{crit}}$	$0.5T_{\text{crit}}$	$0.125T_{\text{crit}}$

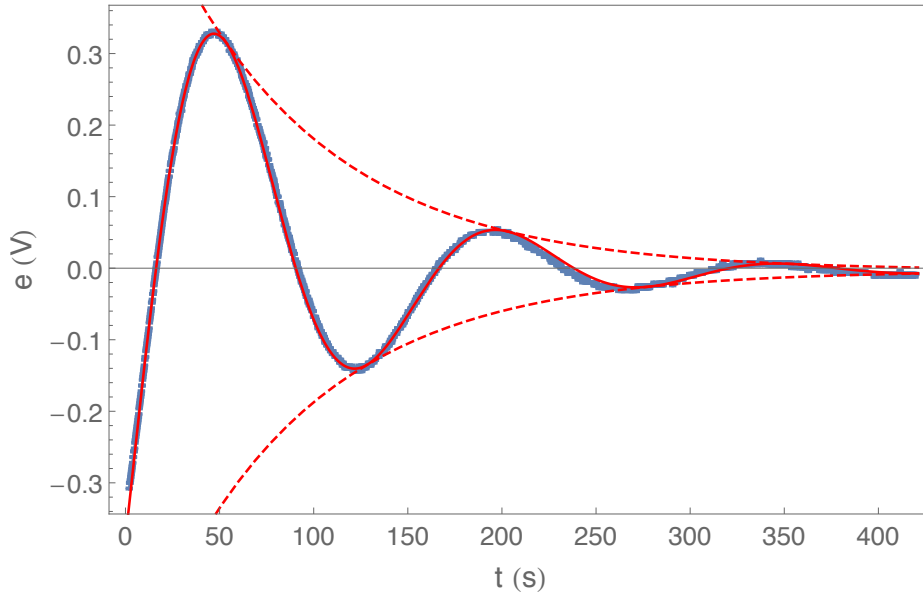


Figure 3.8: Response of the error signal to a step in the control system with a PI-controller. The blue dots show the measurement data with error bars and the red line is the fit. The fit function $A \sin(\omega t - \phi) \exp(-\gamma t)$ is a damped harmonic oscillator with angular frequency ω , amplitude A , phase ϕ and an exponential decay rate γ . The change of temperature was from $T_{\text{init}} = 22.8 \text{ }^\circ\text{C}$ to $T_{\text{final}} = 23.3 \text{ }^\circ\text{C}$.

You can see that the method is also described if the feedback loop just contains a P- or PI-controller. For further reading about feedback systems Ref. [25] is recommended.

Let us show the effect of the integral and derivative term based on our temperature control system. The coefficients can be tuned by four potentiometers on the circuit board of the controller, of which three belong to the gain coefficients and one adjusts an offset of the error signal. The set temperature itself can be changed by a potentiometer on the front panel of the controller and the error signal can be monitored on a scope of which the measurement error was assumed to be $\pm 1 \text{ mV}$. First, the I- and D-term were set to zero and the P-term increased such that after changing the set temperature about 0.1 K the error signal is an oscillation with constant amplitude. The result is shown in Fig. 3.7. The oscillation has not exactly a constant amplitude but is slightly decreasing that indicates a too low gain coefficient. In the beginning the amplitude was, even at the maximum value of k_{P} , decreasing much more. For this reason we had to decrease the internal resistor R442 of the circuit board from initially $10 \text{ k}\Omega$ to $3.24 \text{ k}\Omega$ and therefore could increase k_{P} by a factor of about 3. Because at the maximum value of $k_{\text{P}}^{\text{max}}$ the result in Fig. 3.7 has compared to the periodic time an almost con-

stant amplitude the resistor was not changed again and we assumed $k_P^{\max} = k_{\text{crit}}$. The requirement to change the resistor to get a larger proportional gain than in the beginning could be caused by the large thermal mass of the aluminum block of our system. By fitting a sine function to the data with respect to the measurement error, we determined the critical time to be $T_{\text{crit}} = (51.89 \pm 0.01)$ s. Now the optimum gain coefficients could be set by the Ziegler-Nichols method. Thus k_P can be chosen but unfortunately we do not know an absolute value of the integral and derivative gain, so we had to find the optimum values by trial and error. First the integral gain was increased and the proportional gain decreased which led to an underdamped oscillation as shown in Fig. 3.8. The criterion for optimizing the integral gain was to find a fast decaying oscillation but still short oscillation period. If the integral gain is too low, the system will drift in the long-term. For our system the optimum value of k_I was found to be a potentiometer position of about 0.7 ± 0.1 , if we assume a potentiometer range $[0, 1]$. At last the derivative

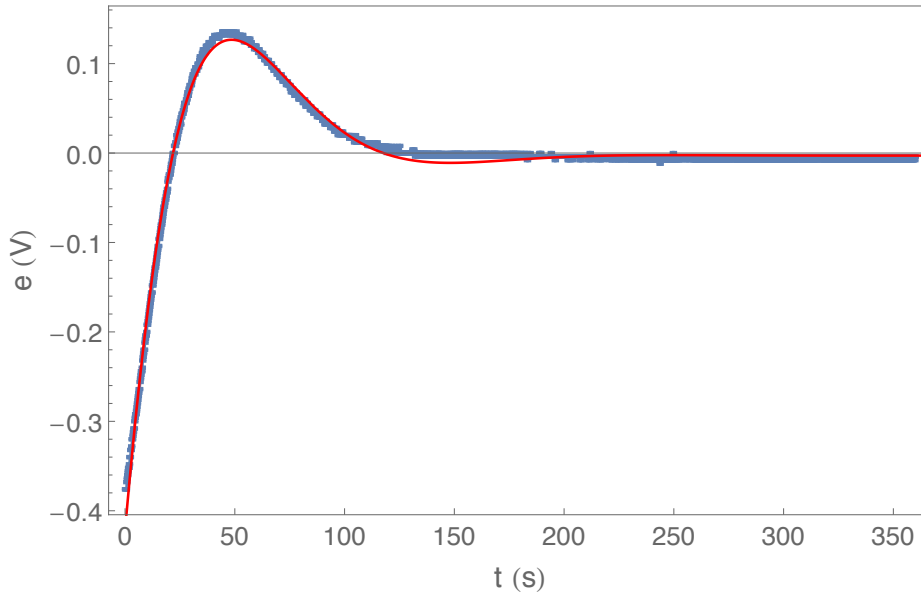


Figure 3.9: Response of the error signal to a step in the control system with a PID-controller. The blue dots show the measurement data with error bars and the red line is the fit. As in Fig. 3.8, a damped harmonic oscillator is the fit function. The change of temperature was from $T_{\text{init}} = 22.8$ °C to $T_{\text{final}} = 23.3$ °C.

term has to be set. When this term is turned on, the damping of the oscillation increases where a too large value of k_D leads to an overdamped oscillation of the error signal and to a very slow convergence to the steady state. The derivative term was carefully increased until the oscillation was critically damped ideally. In our case also k_P and k_I were fine-tuned to find the best parameters where the system reacts fast to a temperature change and reaches the equilibrium in a short

time while maintaining a long-term stability. The best parameters normalized to the maximum value of the potentiometer scale are found to be

$$\frac{k_P}{k_P^{\max}} = 0.7 \pm 0.1, \quad \frac{k_I}{k_I^{\max}} = 0.7 \pm 0.1, \quad \frac{k_D}{k_D^{\max}} = 0.25 \pm 0.1 \quad (3.2)$$

The error signal of the optimized PID temperature controller of the laser is shown in Fig. 3.9. From the exponential envelope of the fitted damped oscillator, the time τ when the error $|e(t > \tau)| < 10$ mV resp. the difference between the set and actual temperature $|T_{\text{set}} - T_{\text{act}}| < 10$ mK is $\tau = (151.1_{-0.7}^{+5.6})$ s. The errors are not only due to the measurement error of the scope but also to the time I needed to enter the set temperature and adjust the scope time to zero.

Chapter 4

Optical setup

In this chapter the optical setup outside of the laser cavity is described. The aim is to couple the laser beam with high efficiency into optical fibers that can transmit light between the optical tables. A small amount of light is coupled into a fiber which is connected to the wavemeter to determine the wavelength of the laser. Most of the power is fed into another fiber that is later used for the experiment. First I will discuss some general features of the optical setup shown in Fig. 4.1. Afterwards I discuss anamorphic prism pairs that I mounted to shape the beam of my laser. An accurate beam shape is required for efficient fiber coupling [12, 16].

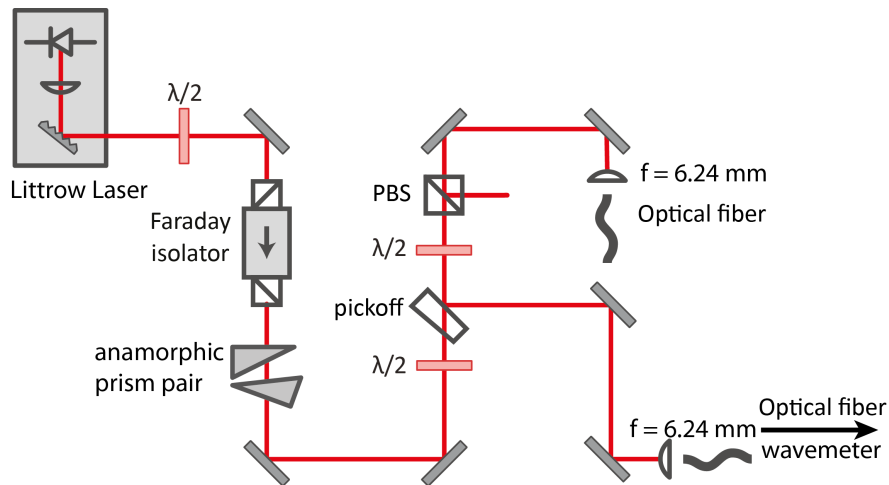


Figure 4.1: The optical setup on the bread board where the laser cavity is mounted. The optics should shape the beam provide two fiber ports.

4.1 General Features

Here, I would like to present some features that can be found in most of the optical setups. With this knowledge the reader can already get an orientation in the zoo of optics in a laboratory.

$\lambda/2$ -waveplate The electromagnetic wave emitted by a laser has a defined polarization. A $\lambda/2$ -waveplate consists of a double-refracting crystal that has an anisotropic structure with one axis preferred that we call the optical axis. This anisotropy leads to an index of refraction that depends on the polarization of the propagating light. The crystal of the waveplate is cut in such a way that its optical axis lies in the plane of the waveplate. The polarization of the incoming light is after traveling through the waveplate mirrored on the plane defined by the optical axis. By rotating the waveplate, the optical axis rotates and therefore the change in angle of the incoming and outgoing light can be chosen. Thus, an arbitrary linear polarization can be obtained.

Polarizing Beam Splitter A PBS splits light into its s- and p-polarized parts. The polarization selecting element is a dielectric coating that transmits light with e.g. p-polarization and reflects light with s-polarization at a 90° angle. Usually $\lambda/2$ -waveplates and PBS are used in combination. By putting the waveplate in front of the PBS the ratio between reflected and transmitted light can be tuned if the waveplate is rotated.

Optical Isolator An optical isolator is the counterpart of an electrical diode because light can only be transmitted in one direction and light traveling the opposite direction is blocked. The optical isolator is required to protect the laser diode from undesired back-reflections that can occur on optical elements. The physical effect behind an optical isolator is the Faraday effect. By applying a magnetic field to a material, the symmetry can be broken and the index of refraction differs between left- and right-circularly polarized light. If linear polarized light propagates through this medium the polarization is rotated by an angle that depends on the magnetic field, the traveled distance and the material-specific Verdet constant. The direction of rotation does not depend on the direction of propagation of the light. Thus, the polarization of a light wave is rotated by 45° , for instance, during propagation through the medium. By putting a mirror behind the optical isolator, the light now propagates in the other direction. The polarization is again rotated in the same direction as before and now is perpendicular to the one in the beginning. If a polarization filter parallel to the incoming wave is put in front of the medium and another filter rotated by 45° at the back, an optical isolator is created. The light from one direction is transmitted where light coming from the other direction hits the polarization filter with an angle of

90° and cannot pass the isolator.

Fiber coupling An optical fiber is an element that can guide light along its path ideally without any losses. Fibers have become integral parts in communication technology due to pioneering developments in the last decades. The idea can be understood by geometrical optics. If a ray of light coming from an optical medium with refractive index n_1 hits the surface of a different optical medium with n_2 and furthermore $n_1 > n_2$, then the ray is reflected and not transmitted if the angle of incidence $\theta > \arcsin \frac{n_2}{n_1}$ that is simply given by Snell's law. This effect is the so-called total internal reflection. An optical fiber is using this physical effect by consisting of two different glasses resp. indices of refraction. The inner core has a lower refractive index than the cladding layer and the light that fulfills the condition for total internal reflection is guided along the fiber. If we now go one step further and think about electromagnetic waves, the Maxwell equations have to hold for light in the fiber. This means that the electromagnetic field distribution in the fiber is given by solutions of the Maxwell equations that fulfill the boundary conditions given by the refractive materials and dimensions of the glass layers. This solutions are called the eigenmodes of the optical fiber and are given by the Bessel functions if we assume a step-like profile of the refractive index and a cladding layer whose radius is much larger than the wavelength. A derivation of the eigenmodes can be found in Ref. [12]. The number of solutions is determined by the radius of the core. If there is just one solution, the fiber is said to be single-mode, if there are more than one, it is called multi-mode. The advantage of single-mode fibers is that the light emitted from the fiber is in the lowest order gaussian mode that we will get to know later in Ch. 5.1.1. But to have light emission from the fiber, the light first has to be coupled into the fiber on the other end. Because the core of a single-mode fiber has a diameter of just a few μm this has to be done by a precise alignment. The coupling efficiency is determined by the overlap integral of the mode of the incoming beam and the eigenmode of the fiber. Since the characteristic size of the mode is given by the core's diameter, the beam first has to be focused. This can be done with an aspherical lens with a short focal length. Because the fiber has a cylindrical symmetry, the eigenmode is rotationally invariant. Thus the profile of the incoming laser beam has to be circular to maximize the overlap integral. Therefore the beam has to be shaped which can be done using an anamorphic prism that is discussed in the next section.

4.2 Anamorphic Prism Pair

A pair of prisms can be used to change the diameter of the beam along one axis while the other axis remains unaffected. Because of the shape of a prism the light has to pass different optical path lengths and thus the diameter of the beam can

be either compressed or expanded. Let us first consider a transition of a beam from a medium with refraction index n_1 into a medium with index n_2 . As shown in Fig. 4.2a the incident beam has diameter d_1 and an angle of incidence ϵ . The

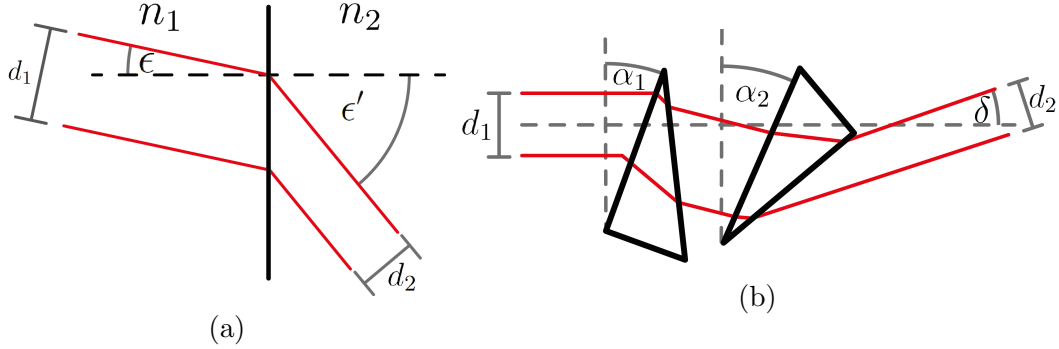


Figure 4.2: The incoming beam has diameter d_1 and the outgoing beam has diameter d_2 . Panel (a) shows the transition of a beam from one medium to another. The diameter of the beam changes dependent on the angle of incidence. Panel (b) shows the situation for a prism pair. The functional relation between those is depend on all four diffractions.

diameter d_2 of the transmitted beam is then given by

$$d_2 = d_1 \frac{\cos \epsilon'}{\cos \epsilon} = d_1 \frac{\cos \arcsin \left(\frac{n_1}{n_2} \sin \epsilon \right)}{\cos \epsilon}, \quad (4.1)$$

where ϵ' is the angle of diffraction and Snell's law, $n_1 \sin \epsilon = n_2 \sin \epsilon'$, is used [16]. For the situation of the prism pair, Eqn. (4.1) has to be applied for four surfaces where the angles of incidence have to take the position of the prisms into account. These positions should be described by the angle to the normal of the optical axis and prism's surface as you can see in Fig. 4.2b. The ratio between the beam diameters is defined as the magnification $M = \frac{d_2}{d_1}$. This magnification M has in general a complicated form and because it would not bring a huge benefit to show it here, the formula can be found in appendix C. Instead we concentrate on the result. In Fig. 4.3a we plot the magnification factor M in dependence on the angle α_2 for different angles α_1 . You can see that the magnification grows approximately linearly for angles up to about 20° while keeping α_1 fixed. For larger angles correspondingly larger magnifications the gradient increases and even starts to diverge which is due to total internal reflection. Moreover, the choice of angles is not unique. Fig. 4.3a shows the angle δ which we would like to be near zero because this means the trace of the beam is just shifted but has still the same direction of propagation. This condition might restrict the combination of angles as well as losses due to reflection.

Let us now consider the laser beam coming out of the laser I built. By eye the

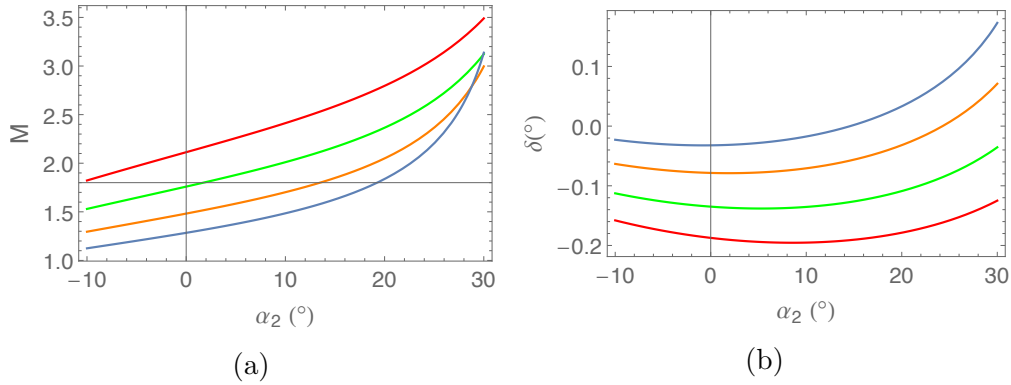


Figure 4.3: The left panel shows the magnification factor of a prism pair and the right panel the angle between the outgoing beam and the optical axis versus α_2 . The refractive indices are assumed to be $n_1 = 1$ and $n_2 = 1.7767$ which is the refractive index of NSF11 glass for $\lambda = 689$ nm. The colors belong to different angles α_1 as follows: Red $\rightarrow -3^\circ$, Green $\rightarrow 0^\circ$, Orange $\rightarrow 5^\circ$ and Blue $\rightarrow 12^\circ$

beam already looked elliptical so that the beam definitely had to be shaped. The beam was first investigated by a CCD camera and the beam profile software *RayCi*. As we will see in Ch. 5.1.1 the divergence of a gaussian beam depends on the width of the beam waist. So the shape of an elliptical beam will change itself while propagating. For this reason the camera was not put directly in front of the laser cavity but in a distance of about 36 cm away from the laser's case (a rough estimation of the distance to the fiber port used later). The observed beam shape without an anamorphic prism pair is shown in Fig. 4.4. The shape of the

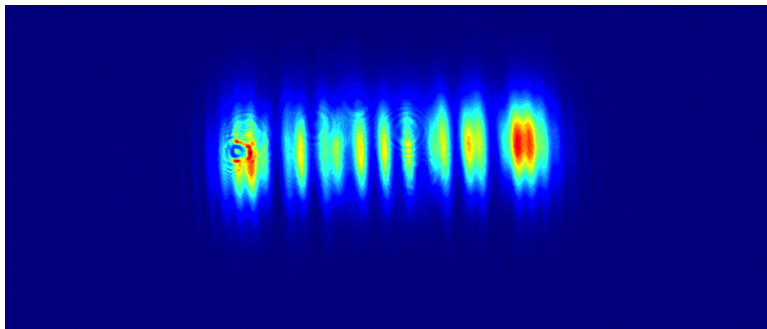


Figure 4.4: The laser beam shape in a distance of ≈ 36 cm from the cavity case detected with a CCD camera. Areas of high intensity are colored in red and areas of low intensity in blue. The diffraction rings might be created by dust on the camera.

beam in the vertical direction looks already nicely gaussian while the horizontal

direction is not just a gaussian intensity profile with broader width than the vertical but it has fringes. This can be indicated by several factors. Firstly, spherical aberration might occur on the (aspherical) collimation lens or on the Brewster window. Secondly, the gaussian beam can lead to a different intensity pattern than expected by Eqn. (2.25) at the grating. Thirdly, the transverse mode of the semiconductor laser diode has the shape shown in Fig. 4.4 that can be due to the small dimensions of the light emitting area related to the wavelength [10]. By compressing the beam, we will have additional effects of interference that occur between the fringes. Note that the considerations about the prism pairs were presented in terms of ray optics. Nevertheless, we can approximate a collimated gaussian beam as a ray in geometrical optics. Unfortunately the mode of our beam is not very gaussian, so I had to find optimum position of the prisms by observing the beam shape on the camera. Fig. 4.5 shows the result which was again observed by the beam camera at the same distance as before. Now the gaussian mode can be seen in both the horizontal as well as the vertical direction. A gaussian fit was made by the beam profile software which gives a major width

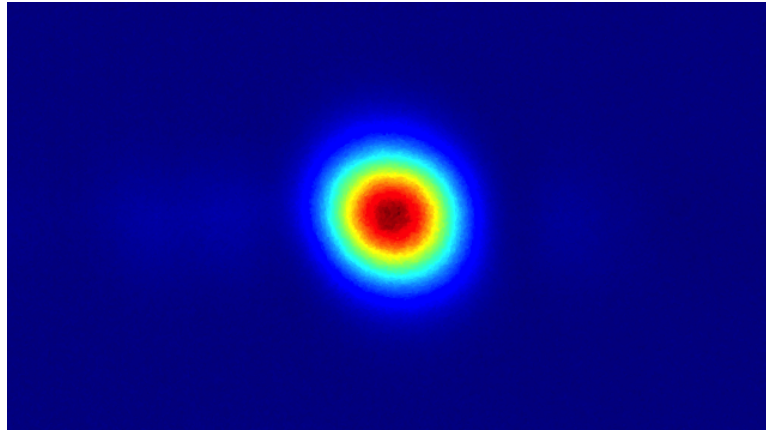


Figure 4.5: The shape of the laser beam in distance of ≈ 36 cm from the cavity case. Here a self-mounted prism pair was put in the beam's path. The ellipticity of the gaussian fits is $\epsilon = 0.917$

$w_{\text{major}} = 0.807$ mm and a minor width $w_{\text{minor}} = 0.740$ mm that describe the full width where the intensity decreased by a factor of $1/e^2$ with respect to the peak intensity. This corresponds to an ellipticity of $\epsilon := \frac{w_{\text{minor}}}{w_{\text{major}}} = 0.917$. The beam could be shaped to an almost circular gaussian mode that is an important requirement for a high coupling efficiency into the fiber. After the beam was shaped, the final position of prism's angles are $\alpha_1 \approx 0^\circ$ and $\alpha_2 \approx 25^\circ$. The plots in Fig. 4.3b predict a magnification of 2.5 – 3 for this values. From Fig. 4.4 we would expect a magnification in the range 4 – 5 and thus we can see that the fringes of the initial beam are not negligible in our case. To conclude, a formula

for the expansion and compression of ray was derived and is expected to hold for collimated gaussian beams. For beams that differ due to e.g. aberrations, the model would have to be extended. The self-mounted prism pair was able to shape the beam profile to a gaussian beam by optimization of the angles and a transmission of 95.5% could be reached. Combined with the use of an aspherical lens with $f = 6.24$ mm, we obtain a fiber coupling efficiency of 60%. This result is satisfying but might still be optimized by the use of a different lens. Since the efficiency was reached with both a $f = 6.24$ mm and $f = 5.0$ mm lens, it leads to the assumption that the optimum fiber coupling efficiency can be reached by a lens with a focal length in between.

Chapter 5

Performance of the Laser

The Littrow laser I built during my Bachelor's project will later be a part of the Strontium experiment. The laser has to work properly in terms of a stable wavelength and a narrow linewidth. Towards these goals, the external noise was reduced by prevention of temperature fluctuations with the PID temperature controller discussed in Ch. 3.9.2, filtering of high frequency noise in the current by the protection board described in Ch. 3.5.2 and damping of vibrations of the external cavity by the choice of the design [1]. At last the light emitted from the laser should be analyzed with regard to its frequency spectrum.

5.1 Mode-Hop-free Tuning Range

A coherent beam of radiation from a laser will only be emitted if the gain medium is within an optical resonator (Ch. 2.3). The resonator then also works as a frequency selective element. In our case, if the grating arm is scanned by the piezo to scan the wavelength of the laser, the properties of the cavity change and the laser can jump to a non-desired wavelength. This is called a mode-hop. We discuss in the following section where the additional frequency selection of the cavity comes from and how mode-hops are suppressed in my laser.

5.1.1 Optical Resonators and Gaussian Beams

Optical resonators are formed by two mirrors and characterized by the curvatures of the mirrors ρ_i , their reflectivities R_i and the distance L between the mirrors. If light enters the cavity, it is reflected on both ends and travels back and forth. Because light is an electromagnetic wave, boundary conditions given by the mirrors have to be fulfilled. Two plane mirrors form a so-called Fabry-Pérot-Etalon [12, 16]. For ideal mirrors with reflectivity $R = 1$, the electromagnetic wave has to vanish at the ends of the cavity and a standing-wave is created. This boundary

condition can be written as

$$m\frac{\lambda}{2} = L \quad \Leftrightarrow \quad \nu_m = m\frac{c}{2L}, \quad m \in \mathbb{N}, \quad (5.1)$$

where λ is the wavelength, ν the frequency of the electromagnetic wave and c the speed of light, and we used $c = \lambda\nu$. This shows that only a discrete spectrum of waves are in resonance with the cavity. Moreover, we define the distance between two resonance frequency as the free spectral range:

$$\Delta\nu_{\text{fsr}} = \frac{c}{2L} \quad (\text{Free Spectral Range}) \quad (5.2)$$

The different resonance frequencies ν_m are associated with the longitudinal modes of the cavity.

Let us consider the more realistic model of two mirrors with finite reflectivity R . To calculate the transmittance T of the cavity we have to take interference into account. An electromagnetic wave $E(\tau, x) = E_0 \exp[i(\omega\tau - kx)]$ enters the cavity. After each round trip in the cavity the wave gets a phase factor of $\exp(-2ikL)$ and the amplitude is lowered because of the finite reflectivity of the mirrors. Thus, the wave after one round trip reads $E(\tau, x) = E_0 r^2 t \exp[i(\omega\tau - kx - 2kL)]$, where r and t are the complex reflectivity and transmittance coefficients with $|r|^2 = R$ and $|t|^2 = T$. The wave then gets reflected again and after a second round trip it reads $E(\tau, x) = E_0 r^4 t \exp[i(\omega\tau - kx - 4kL)]$ and so forth. The transmitted wave in the steady-state is therefore an interference of infinitely many reflected waves in the cavity,

$$E(\tau, x) = E_0 t^2 \exp[i(\omega\tau - kx)] \sum_{n=0}^{\infty} r^{2n} \exp(-2inkL), \quad (5.3)$$

where the additional factor t comes from the transmission when the wave is leaving the cavity. The sum can be evaluated for $|r^2 \exp(-2ikL)| < 1$ by the geometric series and we find

$$E(\tau, x) = E_0 t^2 \exp[i(\omega\tau - kx)] \frac{1}{1 - |r|^2 \exp(-2ikL)}. \quad (5.4)$$

Because the physical observable is the intensity, we are interested in this quantity and calculate

$$\frac{I}{I_0} = \frac{|E|^2}{|E_0|^2} = \frac{(1 - R)^2}{1 + R^2 - 2R \cos(2kL)} = \frac{1}{1 + \left(\frac{2\mathfrak{F}}{\pi}\right)^2 \sin^2\left(\frac{\pi\nu}{\nu_{\text{fsr}}}\right)}, \quad (5.5)$$

where we used $1 - R = T$, the free spectral range (Eqn. 5.2) and defined the Finesse

$$\mathfrak{F} := \frac{\pi\sqrt{R}}{1 - R} \quad (\text{Finesse}). \quad (5.6)$$

We see that the normalized transmitted intensity through a Fabry-Pérot-Etalon is described by an Airy function in frequency space. The Finesse is an important characteristic for cavities and is best illustrated by a plot of the Airy function for different \mathfrak{F} as shown in Fig. 5.1. The Finesse corresponds to the width of the peaks in the intensity pattern where a high finesse is correlated to narrow peaks and thus a precise frequency selection. A high finesse can be reached by high reflectivities of the mirrors.

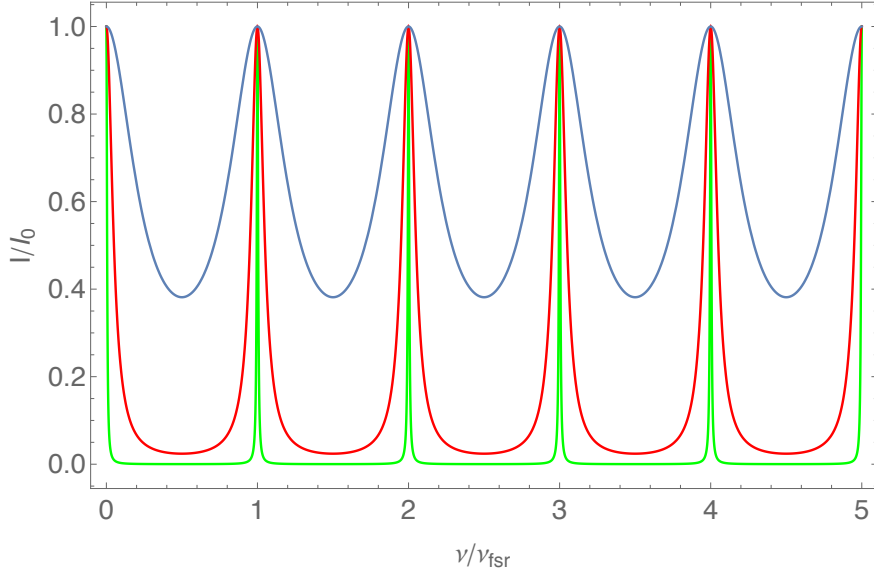


Figure 5.1: The transmitted intensity of a Fabry-Pérot-Etalon in frequency space for different values of the Finesse \mathfrak{F} . For the blue plot $\mathfrak{F} = 2$, for the red plot $\mathfrak{F} = 10$ and the green plot shows $\mathfrak{F} = 100$. The distance between two peaks is the free spectral range ν_{fsr} .

Now we want to consider mirrors that are not flat but instead mirrors with radius of curvature $\rho_0 := \rho_1 = -\rho_2 = L$, where L is again the cavity length at the optical axis. This is a so-called confocal cavity. Because laser beams are not infinitely extended waves but are spatially confined, we briefly discuss gaussian beams in the following to find the resonance condition for the confocal cavity later on. Gaussian beams are solutions of the Maxwell equations in the paraxial approximation and especially describe laser beams. They are assumed to change much slower in the transverse x -, y -direction than in the axial z -direction. The lowest order solution has a gaussian intensity profile in the x and y direction centered at the optical axis and is equated to a “gaussian beam” in this thesis. The functional form of the electrical field is given by

$$E(\mathbf{r}) = E_0 \frac{w_0}{w(z)} \exp \left[-\frac{(x^2 + y^2)}{w^2(z)} \right] \exp \left[-ikz - ik \frac{(x^2 + y^2)}{2\rho(z)} + i\zeta(z) \right] \quad (5.7)$$

Let us introduce the new variables step by step. The spatial extension in the x and y directions of the beam is given by the beam width $w(z)$. This width is the distance from the optical axis where the beam intensity decreased to $1/e^2$ with respect to the peak intensity. The beam width $w(z)$ varies in the z direction with

$$w(z) = w_0 \sqrt{1 + \left(\frac{z}{z_0}\right)^2}, \quad (5.8)$$

where w_0 is the beam waist and thus the tightest beam width is at $z = 0$. Furthermore z_0 is the Rayleigh range and at $z = z_0$ the width has increased by a factor of $\sqrt{2}$. The beam waist and Rayleigh range are related by

$$w_0^2 = \frac{\lambda z_0}{\pi}. \quad (5.9)$$

For $z \ll z_0$ the beam width Eqn. (5.8) can be approximated by $w(z) \approx \frac{w_0}{z_0} z$ and we see that the size of the beam increases linearly with a divergence angle of $\tan \theta_{\text{div}} = \frac{w_0}{z_0} = \frac{\lambda}{\pi w_0}$. So if the beam is focused to a smaller beam waist it diverges more. The wavefront, which is the surface of constant phase of the electromagnetic wave, is curved. The radius of curvature is given by

$$\rho(z) = z \left[1 + \left(\frac{z_0}{z}\right)^2 \right]. \quad (5.10)$$

At the position of the beam waist ($z = 0$) the radius of curvature diverges and the wavefront is a plane. For $|z| > 0$, $\rho(z)$ gets more curved and for $z \rightarrow \infty$ the wavefront becomes a spherical wave. The phase is also shifted in the direction of propagation by the Gouy phase

$$\zeta(z) = \tan^{-1} \frac{z}{z_0}. \quad (5.11)$$

Within the the Rayleigh range from $-z_0$ to z_0 the phase gets an additional shift of $\pi/2$. A detailed description of gaussian beams and effects of optical elements on it, can be found in the review Ref. [26].

Let us apply this knowledge about gaussian beams to find the resonance conditions for the confocal cavity and the profile of the gaussian beam within the resonator that is sketched in Fig. 5.2.

The boundary conditions are easy to find. Because the electrical field has to vanish on the mirrors, the wavefront has to coincide with the curved mirrors. So we know that $\rho(z) = \rho_0$ and from this condition we already can calculate the other parameters of the beam. From $\rho(z)$ we get the Rayleigh range and from this the waist radius, and thus everything is defined:

$$z_0 = \frac{L}{2}, \quad w_0^2 = \frac{\lambda L}{2\pi} \quad (\text{Confocal cavity}) \quad (5.12)$$

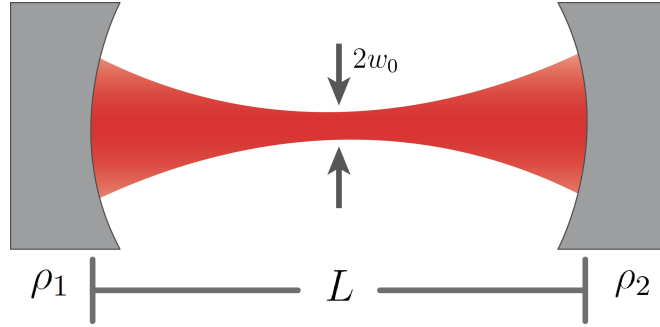


Figure 5.2: The figure shows two curved mirrors that form a resonator. The mode of the cavity is a gaussian beam. For a confocal cavity it holds $\rho_1 = \rho_2 = L$.

At last we have to consider the phase to find the resonance conditions. To have a standing wave in steady-state, the phase has to be the same after each round trip. From our boundary condition we know that the phase is the same on the surface of the mirrors, so we can calculate the phase shift of a round trip on an arbitrary point, so we choose the optical axis where $x = y = 0$. By Eqn. (5.7) the phase shift is given by twice the propagation to the other end of the cavity, and we get $2kL - 2\Delta\zeta$ and $\Delta\zeta = \zeta(L/2) - \zeta(-L/2) = \pi/2$. To get a standing wave, the phase has to change by a multiple of 2π and we obtain for the resonance frequencies

$$2kL - \pi = m2\pi \quad \Leftrightarrow \quad \nu_m = \left(m + \frac{1}{2}\right)\nu_{\text{fsr}}, \quad m \in \mathbb{Z}. \quad (5.13)$$

Again our free spectral range is $\nu_{\text{fsr}} = \frac{c}{2L}$ which is the distance between the resonance peaks. Compared to the Fabry-Pérot-Etalon, the peaks are shifted by a constant value in frequency space.

If the same considerations are done for higher transverse modes than the gaussian mode one can find that additional resonance frequencies appear. In a confocal cavity, we find

$$\nu_{l,n,m} = m\nu_{\text{fsr}} + (l + n + 1)\frac{\nu_{\text{fsr}}}{2}, \quad (5.14)$$

where the indices l, n count the higher order transverse modes. A deeper insight to cavities is presented in Ref. [12]. In the next section a confocal cavity is used to optimize the mode-hop free tuning range and later the linewidth of the laser is compared to a cavity.

5.1.2 Optimization of the Mode-Hop-free Tuning Range

With the knowledge about resonators we can understand why the longitudinal mode of the laser can suddenly hop to a different mode when the piezo at the grating arm is scanned. By scanning the piezo, not only the angle of incidence to

the grating changes but also the length of the external cavity varies slightly and thus the resonance frequency shift [27]. To scan the laser smoothly the frequency of the peak intensity of the grating's diffraction order as well as the cavity's resonances have to be displaced by the same frequency interval. Because we cannot control the grating's angle and cavity length independently, the frequency distribution changes differently as you can see in Fig. 5.3. The two different plots show the effect of the rotation of the grating. While the center frequency of the grating is shifted, the cavity resonances are changed much less here and you can see that in Fig. 5.3b suddenly two resonance frequencies now have similar intensities. Because the frequencies which are in resonance give feedback to the laser diode, the laser can run in more than one mode or the lasing frequency can jump. This is called a mode-hop. Because we want the laser to be scanned continuously mode-hops have to be suppressed. To see the mode-hops, I coupled my laser into

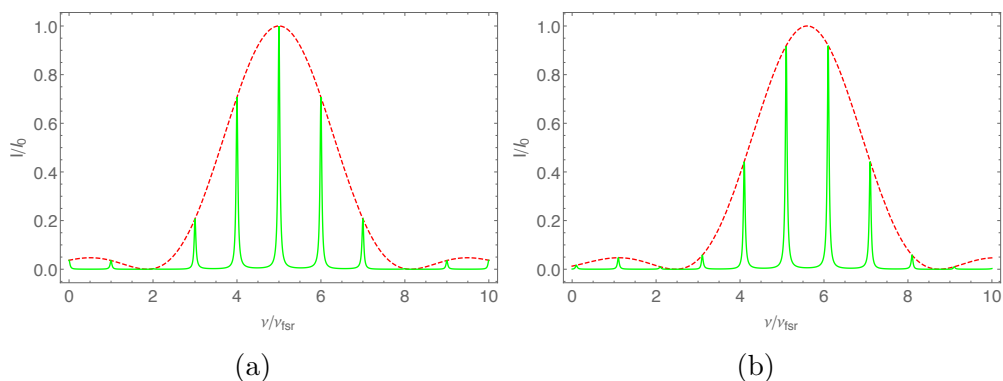


Figure 5.3: The two plots show the frequency selection of the grating and a cavity. The red dashed line is the intensity pattern of a grating and the green line indicates the resulting resonance frequencies of the grating and the cavity. Panel (a) shows the position of the grating in the beginning and panel (b) a rotation of the grating regarding to the Littrow configuration. Here the resonance frequencies shift much slower than the one of the grating.

an additional confocal external cavity with a radius of curvature $\rho_0 = 100$ mm and measured the transmission on a photodiode (*Thorlabs* APD410A2/M). The idea is to then scan the laser as well as the confocal cavity length by a piezo and observe the transmission signal on the scope while the confocal cavity is scanned much faster than the laser. By setting the trigger to the fast cavity modulation, we see a comb of transmission peaks and the slow laser modulation shifts the peaks so that their path on the scope can be followed by eye. If the transmission peaks do jump, a mode-hop is seen.

The optical setup is shown in Fig. 5.4. First the laser beam has to be aligned to the cavity. Because we know the shape of the gaussian mode in the cavity from Eqn. (5.12), we try to form the laser beam as good as possible by lenses

to match the cavity mode. For this, the beam propagation was simulated by the software *GaussianBeam* [28] on the server of our lab and the result was, to use a focal length $f_1 = 6.24$ mm for the fiber out-coupling, and a second lens with $f_2 = 100$ mm at an approximate distance of 30 cm from the first lens to shape the beam. For alignment the cavity length was scanned to be sure to fulfill

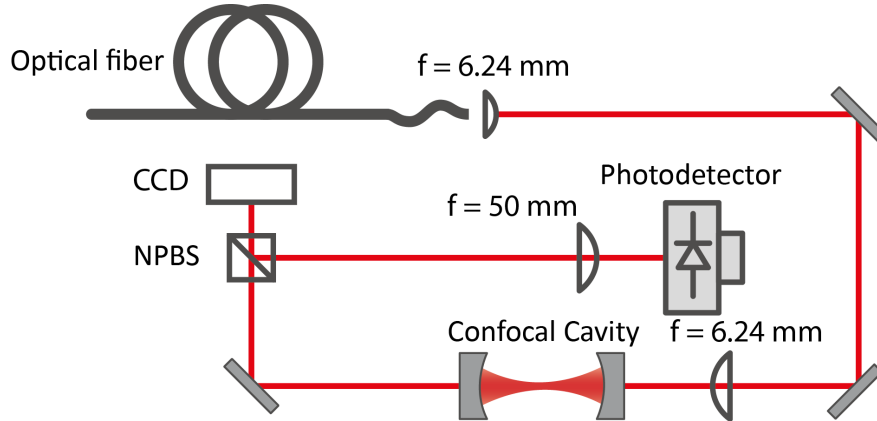


Figure 5.4: The optical setup to couple the laser beam to the cavity and measure the transmission signal. Two lenses with $f_1 = 6.24$ mm and $f_2 = 100$ mm are used to shape the beam. For a better signal the photodiode (PD) was put into the focus of a $f = 50$ mm lens. To also observe the beam profile on a CCD, a Non-Polarizing-Beam Splitter (NPBS) divides the beam.

the resonance condition at some time and see transmission. The first signal on the scope shows equidistant peaks while the number increases when the scanning amplitude is increased because then the resonance condition is fulfilled more often within one period. If the beam is observed on the beam profile camera, the beam does not look gaussian because higher order transverse modes can also be seen. Thus, the resonance peaks are given by Eqn. (5.14) with contributions from $l, n \neq 0$ that gives resonances between two peaks of distance ν_{fsr} . To align the cavity now to the lowest order transverse mode with $l = n = 0$, we minimize every second peak on the scope that are odd multiples of $\nu_{\text{fsr}}/2$. This can be seen in Fig. 5.5. Once the cavity is aligned, the mode-hop-free tuning range can be determined. For this measurement, the cavity was scanned with an amplitude chosen such that two peaks can be seen within one period and the scope was triggered with this frequency. Then the amplitude of the piezo in the laser cavity was increased and the peaks began to shift on the scope. Every time a mode-hop happens the peaks jump. If the laser scanning amplitude is increased, the grating will be rotated by a greater angle and more mode-hops are observed. As described above, we have to suppress the mode-hops and we can do this by changing the parameters temperature T and current I . The temperature affects the cavity length and the refractive index of the semiconductor laser diode de-

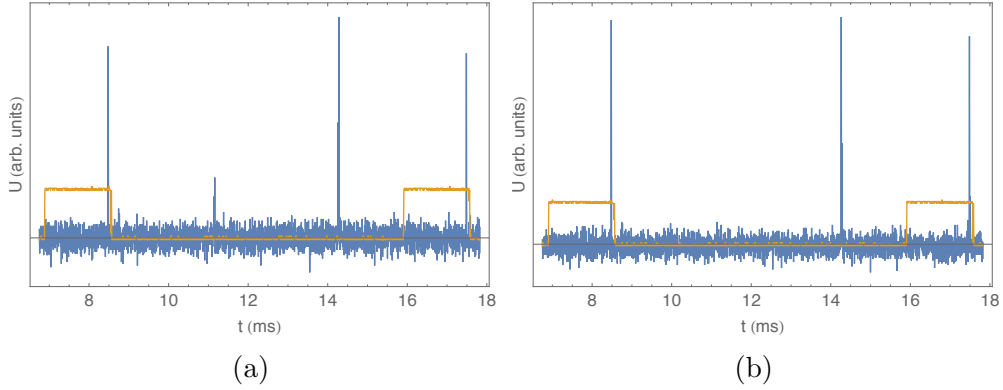


Figure 5.5: The picture on the scope where the blue line corresponds to the photodiode signal and the orange one is the trigger signal of the cavity length scanning piezo. The blue peaks between the two orange steps are the resonance peaks when the voltage is ramped up. The peaks where the step of the orange signal is, appear because the voltage on the piezo is ramped down in a faster time than ramping up but still in a finite time. In panel (a) you see the situation where higher transverse modes are excited in the cavity. After aligning those higher modes can be suppressed and only the peak that belongs to a even multiple of $\nu_{\text{fsr}}/2$ survives as you can see in panel (b).

depends on temperature and therefore also on the current. A change in T and I affect therefore the optical length of the cavity [22]. The idea is to simultaneously modulate the voltage applied to the piezo and the current running through the laser diode with the help of a feed-forward system in the scan controller. An internal setting on the *Toptica SC 110* controller was tuned which determines how much the current is changed for a certain piezo voltage. My procedure was to step-by-step increase the amplitude of the piezo until mode-hops appear on the scope. If the mode-hops could not be removed by tuning the offset of the piezo voltage, the feed-forward was tuned until the laser frequency was scanned continuously. Then again the amplitude was increased and the procedure repeated. If the mode-hops could not be suppressed by the feed-forward, the set current on the current controller was changed. All steps were iterated for different currents and piezo offset voltages. As soon as the settings with the largest piezo amplitude of the laser were found, the wavelength was observed on a wavemeter. To center the scanned interval around the desired wavelength of $\lambda = 689.4487$ nm, the temperature was taken into account. By increasing the temperature the lasing center wavelength also increases because at a higher temperature the optical path length in the cavity is larger. If we think about the boundary condition of a Fabry-Pérot-Etalon (Eqn. 5.1), the resonance wavelength is proportional to the cavity length. Obviously by changing the temperature to center the wavelength, the feed-forward and current have to be adjusted again slightly. In the end, the

frequency interval that can be scanned without having a mode-hop was read out on the wavemeter. I was able to optimize the mode-hop-free tuning range up to (15.3 ± 0.05) GHz @ $T_{\text{set}} = (20.3 \pm 0.05)$ °C and @ $I_{\text{set}} = (148 \pm 0.5)$ mA. The error of the mode-hop-free tuning range is due to drifts on the MHz scale. They probably appear because the system is not thermalized while scanning which leads to fluctuations. The errors of the temperature and current are because the values on the *Toptica* controller are rounded to finite digits. The set current was read-out on the *Toptica* controller and is not the same as the current flowing through the laser diode because of the protection board (Ch. 3.5.2).

5.2 Linewidth

As a final step the frequency spectrum of the laser was analyzed. The spectrum of a laser is often assumed to be monochromatic but this is an ideal picture. In reality the electromagnetic spectrum of a single-mode laser is a peak around a center wavelength and an usual characteristic value of a laser's performance is the linewidth that is the FWHM of this peak. In the following the linewidth was measured by two different methods and compared to a commercial *Toptica* narrow-linewidth 689 nm laser.

5.2.1 Linewidth Measurement with a Cavity

The first method to measure the linewidth uses the confocal cavity described in Ch. 5.1.2. For a high Finesse \mathfrak{F} the peaks of Eqn. (5.5) can be approximated by a comb of lorentzian functions. Let us assume that the linewidth of the laser is also a lorentzian function. This is valid because in Litrow lasers the allowed lasing frequencies are determined by the external cavity. A lorentzian function $g(\nu)$ is given by

$$g(\nu) = \frac{1}{\pi} \frac{\Delta\nu/2}{(\nu - \nu_0)^2 + (\Delta\nu/2)^2}, \quad (5.15)$$

where the center angular frequency is at ν_0 and $\Delta\nu$ is the FWHM. If the confocal cavity is scanned in length, the resonance peaks shift back and forth in frequency space. If the laser is mode-matched to the cavity and the transmission is observed, then the Airy function resonance shape of the cavity is shifted across the lorentzian line shape of the laser in frequency space. The measured intensity spectrum is the convolution of the laser's and cavity's linewidth. Since we can approximate the peaks of the Airy function by lorentzians, this convolution is again a lorentzian function but with $\Delta\nu = \Delta\nu_{\text{laser}} + \Delta\nu_{\text{cavity}}$ and $\nu_0 = \nu_{0,\text{laser}} + \nu_{0,\text{cavity}}$. To determine the linewidth of the laser I built, the linewidth or Finesse of the confocal cavity is required which has to be measured first. Thus, I used a commercial *Toptica* laser that also runs at a wavelength of 689 nm where the datasheet promises a linewidth of < 50 kHz. For the measurement, the piezo of the confocal cavity was

modulated with a frequency of about 13 Hz and the amplitude was low enough to see just two resonance peaks. This should minimize the error that occurs from the hysteresis of the piezo but we required at least two resonances to determine the free spectral range and therefore to have a scale to convert from time to frequency units. Figure 5.6 shows the result of this measurement with a lorentzian function fitted. The width of the lorentzian is $\Delta\nu_{\text{Optica}} = (1.61^{+0.084}_{-0.078})$ MHz. There are

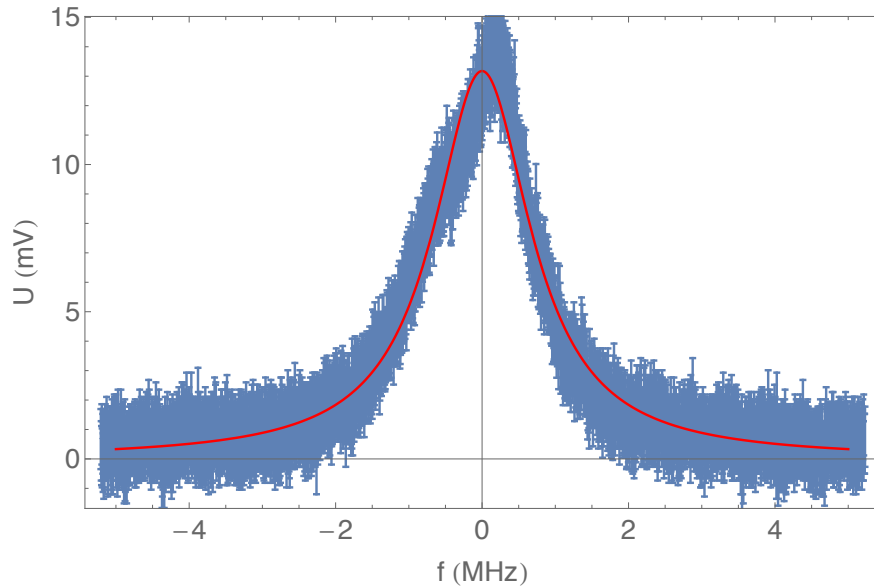


Figure 5.6: The plot shows the photodiode signal of the transmission through the confocal cavity with a narrow-linewidth laser. The model for the fit function is a lorentzian whose FWHM was determined to be $\Delta\nu = (1.61^{+0.084}_{-0.078})$ MHz.

different errors in this measurement. First, we have the measurement errors of the scope that were assumed to be ± 1 mV. Second *Thorlabs* predicts a relative error of the photodiode output signal of $\pm 3\%$. Those two errors are negligible with respect to the third one which is related to the cavity properties. I did not characterize the cavity further and because it is mounted in a brass spacer, the cavity length was only roughly measured so that I assumed $L = (100 \pm 5)$ mm. We can also see from the data points in Fig. 5.6 that the cavity is not perfectly confocal because the peak is slightly asymmetric. An asymmetry would also be justified if the cavity length does not match the radius of curvature of the mirrors. Then the resonance condition Eqn. 5.14 would no-longer be degenerated for even multiples of ν_{fsr} so that the peaks split up. For a small error this leads to asymmetric peaks.

The overlap time of the laser and cavity resonance is approximately $T = 200 \mu\text{s}$, so we should take into account that the results we obtain for the linewidth measurement also depend on the time. From the measured result for the convolution,

we see that the linewidth of the cavity is in the MHz range and the *Toptica* laser which has a linewidth smaller than 50 kHz for $T = 5 \mu\text{s}$ does not contribute a lot to the convolution if we assume that linewidth is still in the 10 kHz range for 200 μs . Let us now compare the result to the same measurement done with the home-built laser. The experimental conditions were identical to the ones above. The measured photodiode signal and the fitted lorentzian are shown in Fig. 5.7. The FWHM of the lorentzian is given by $\Delta\nu_{\text{home-built}} = (1.82^{+0.096}_{-0.086})$ MHz. The errors occur from the same arguments as above. We see that the laser I built has

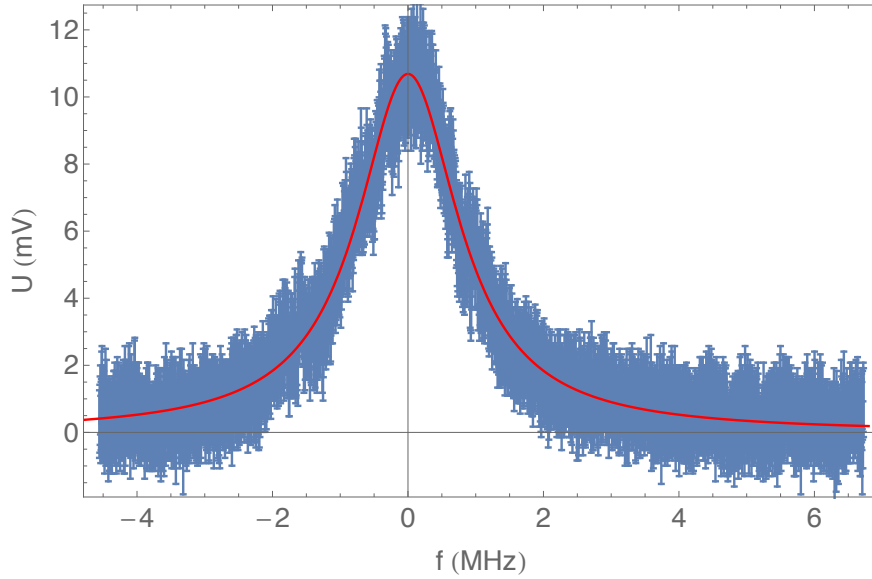


Figure 5.7: The plot shows the photodiode signal of the transmission through the confocal cavity with the laser I built. The fitted lorentzian function has a FWHM $\Delta\nu = (1.82^{+0.096}_{-0.086})$ MHz.

a larger linewidth than the commercial laser. For the difference of the FWHM of the both lasers we get $\delta\nu := \Delta\nu_{\text{selfmade}} - \Delta\nu_{\text{Toptica}} = (212^{+12}_{-8})$ kHz for $T = 200 \mu\text{s}$. The errors from the difference in cavity length do not add up because it is a systematic error in both measurements. If we assume that $\Delta\nu_{\text{Toptica}} \ll 50$ kHz, then $\Delta\nu_{\text{selfmade}} \approx \delta\nu$. In Reference [1] a linewidth of 254 kHz for $T = 100 \mu\text{s}$ was reached for their 689 nm laser which shows that we have a slightly narrower linewidth even for a longer measurement time. Since the grating and mechanical design they use is the same, it might be caused by the different laser diode model that we used.

5.2.2 Heterodyne Linewidth Measurement

In this section, I would like to present an alternative method to measure the linewidth of a laser by forming a beatnote between the beam of the laser I built

and the *Toptica* laser. This means that the two laser beams interfere and the intensity pattern is observed on a photodiode as a function of time. By now we considered the light emitted from a laser as an overlap of a continuous distribution of frequencies. This distribution was assumed to be a lorentzian function with a defined linewidth. Let us now think about a different picture. Here, the laser light is described as a single harmonic wave with one fixed angular frequency ω_0 but with a phase $\phi(t)$ that is dependent on time. Thus the electromagnetic field at a certain position is given by $E(t) = E_0 \cos [\omega_0 t - \phi(t)]$. The counterpart to the linewidth is the jitter of the phase in this picture. Since the total phase change will be different within a shorter or a longer time interval and we transferred this to be a measure of the linewidth, we have to be careful when we talk about the linewidth. A more accurate way is to define the linewidth within a certain interval of measurement time.

If we now overlap two waves with angular frequencies ω_1 and ω_2 , phases $\phi_1(t)$ and $\phi_2(t)$ and for simplicity $E_0 = E_{0,1} = E_{0,2}$, the intensity is

$$\begin{aligned} I(t) &\propto |\cos [\omega_1 t - \phi_1(t)] + \cos [\omega_2 t - \phi_2(t)]|^2 \\ &= A + \cos [(\omega_1 + \omega_2)t - (\phi_1(t) + \phi_2(t))] \\ &\quad + \cos [(\omega_1 - \omega_2)t - (\phi_1(t) - \phi_2(t))], \end{aligned} \quad (5.16)$$

where A summarizes the terms proportional to the intensity of each beam. The second term is a cosine and for optical frequencies ω_1, ω_2 , it is oscillating so fast that it cannot be detected by a photodiode. For small detunings $\Delta\omega = \omega_2 - \omega_1$ the last term can be in the range of radio frequencies and can indeed be detected by fast photodiodes [29]. This method to create new frequencies from two initial frequencies is called the heterodyne technique. What we expect to see on the scope is a sine wave but with perturbations due to the changing phase. To determine the linewidth from this signal, we could observe it with a spectrum analyzer. This analyzer requires a minimal signal duration and because we saw that the linewidth should be specified within a certain time interval, it would have a lower boundary given by the spectrum analyzer. Thus we use a different technique to get the power spectrum. The Wiener-Khinchin theorem states that the power spectral density $\text{PSD}(\nu)$ of our beatnote signal $x(t)$ is the Fourier transform of the autocorrelation function $\Gamma_{xx}(\tau)$ of the signal [30]:

$$\text{PSD}(\nu) = \int_{-\infty}^{+\infty} \Gamma_{xx}(\tau) e^{-2\pi i \nu \tau} d\tau \quad (5.17a)$$

$$\Gamma_{xx}(\tau) := \langle x(t)x^*(t-\tau) \rangle = \lim_{T \rightarrow \infty} \frac{1}{T} \int_0^T x(t)x^*(t-\tau) dt \quad (5.17b)$$

Because in our case the digital scope gives the beatnote signal $x(t)$ as a discrete function the integrals have to be replaced by sums.

The optical setup for our measurement is shown in Fig. 5.8. The two lasers were

also coupled to the wavemeter and the laser I built was tuned by the piezo such that the detuning was in the range of a few ten MHz. Because none of the lasers were locked, the detuning was drifting and had to be readjusted several times. To have a stable beatnote signal on the scope the polarization of the

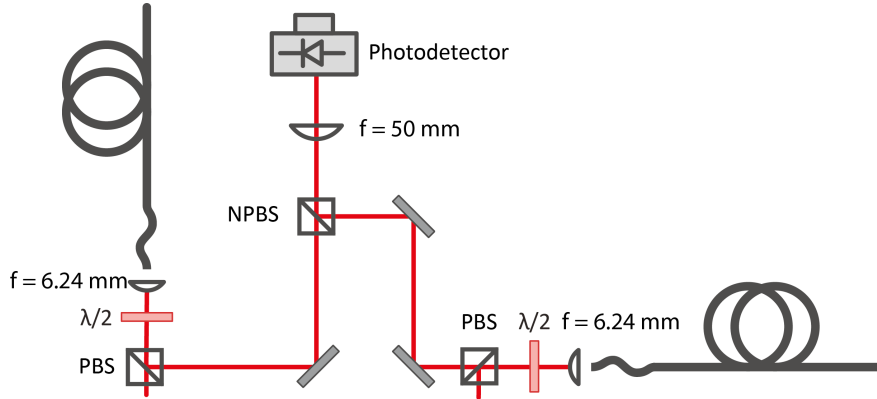


Figure 5.8: The optical setup to detect the beatnote signal. The two beams were overlapped by a NPBS. The $\lambda/2$ -plates and PBS are used to obtain the same intensities in both beams.

light in the polarization-maintaining fibers has to be set correctly otherwise the intensity behind the beam splitter fluctuates. For this purpose, the output power after the PBS can be observed while perturbing the fiber by (say) heating it up with your hands. The waveplate at the fiber in-coupling has to be rotated until ideally no power fluctuations can be seen due to this perturbation. The raw data signal observed on the scope is shown in Fig. 5.9. The beatnote is oscillating with a frequency of the detuning and contains information of both the *Toptica* as well as my home-built laser. By calculating the autocorrelation function of the signal and taking the Fourier transform we get the power spectral density of the beatnote of both lasers. From Eqn. (5.16) we see that the phase fluctuations will add up in the PSD. So if we read the FWHM of the PSD we will have the sum of the linewidths of both lasers. The advantage of this technique is now that we do not have to assume a certain shape of the linewidth as we did in Ch. 5.2.1.

As discussed above the linewidth is a property that has to be defined for an interval of time. For measurement times $T = 50 \mu s$ and $100 \mu s$ the power spectral density centered around the peak position is plotted in Fig 5.10a on a logarithmic scale. As you can see the green line which corresponds to the shorter measurement time is more narrowly peaked than the blue line. This confirms our assumption of the time-dependent linewidth. Obviously the linewidth gets broader if the measurement time is longer because of more fluctuation of the phase. For even longer times we might also expect broadening effects due to drifts of the laser because they are not locked. Figure 5.10b shows again the beatnote signal for

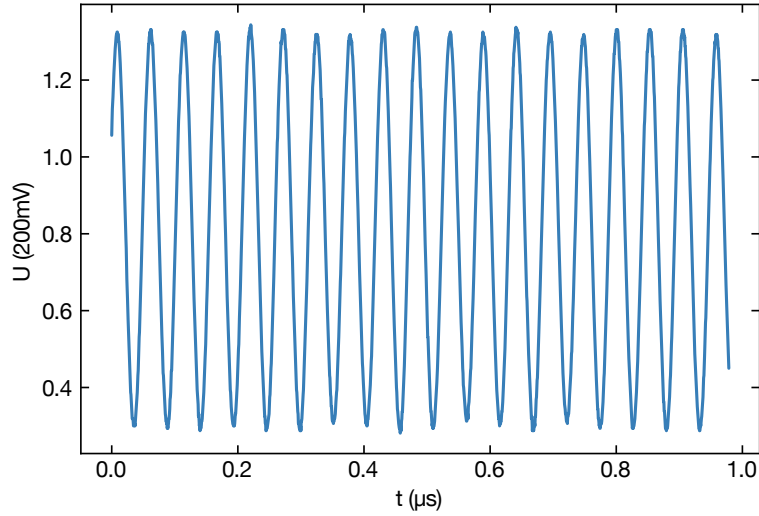
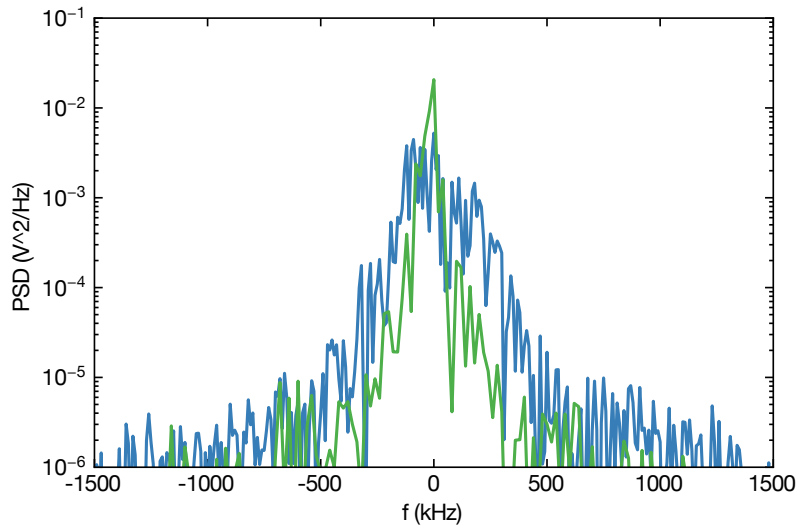
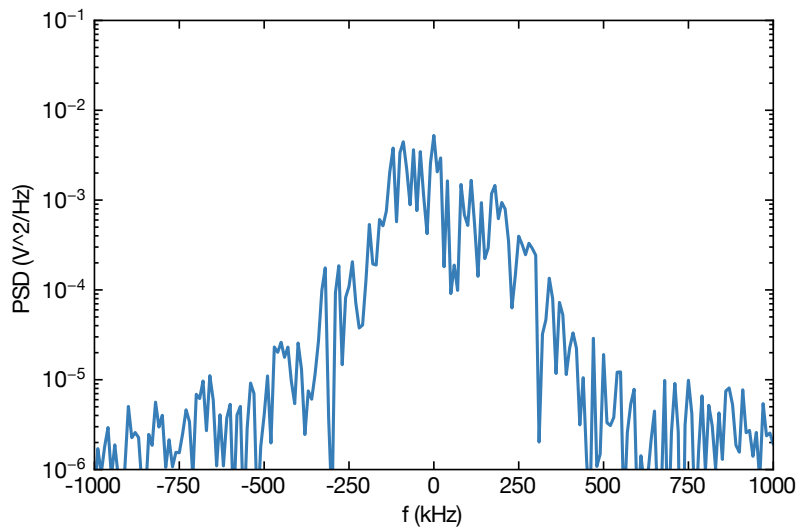


Figure 5.9: The beatnote signal observed on the scope. The sampling rate is 4 GHz.

$T = 100 \mu\text{s}$ but now it is zoomed into the frequency axis to read out the FWHM. Because we do not assume a model of the linewidth, we simply determine the width of the power spectral density where the maximum decreased by a factor of two. Be aware that the plots have a logarithmic scale on the power axis and thus the factor between the peak maximum and noise is about 10 000. By reading out the FWHM on the plot we get $\Delta\nu = (127.8 \pm 14.4) \text{ kHz}$ for a measurement time of $T = 100 \mu\text{s}$. If we gain assume the spectral width of the reference laser to be much narrower, then $\Delta\nu$ corresponds to the laser I built. The linewidth $\Delta\nu$ is an average over the results of ten single measurements with $T = 100 \mu\text{s}$. The error is on one hand due to reading out the FWHM and on the other hand due to the sampling rate of the scope. This sampling rate is 4 GHz and therefore the maximum resolved frequency of the PSD is 2 GHz that is given by the discrete Fourier transform. This range of 2 GHz is itself divided into $4 \text{ GHz} \cdot 100 \mu\text{s} = 4 \cdot 10^5$ data points distanced at $2 \text{ GHz} \cdot (4 \cdot 10^5)^{-1} = 5 \text{ kHz}$ which is then resolution bandwidth for $100 \mu\text{s}$. This finite resolution also did not allow me to measure the linewidth reasonable for shorter times to then compare it to the *Toptica* laser from which we know the linewidth for $T = 5 \mu\text{s}$. The result of the beatnote measurement shows a linewidth that is half the linewidth we found by convolving with the cavity's resonances. This can be explained by the different measurement times of $T = 200 \mu\text{s}$ for the cavity method and $T = 100 \mu\text{s}$ for the heterodyne technique.



(a) The green line corresponds to a measurement time of $T = 50 \mu\text{s}$ and the blue line to $T = 100 \mu\text{s}$. The graphs are centered around their peak position.



(b) The PSD for a measurement time of $T = 100 \mu\text{s}$. The scale of the frequency axis is smaller than in Fig. 5.10a.

Figure 5.10: The power spectral density of the beatnote signal for different measurement times and magnification of the frequency axis. The data evaluation was done with the help of the Python SciPy library that includes the function “signal.periodogram” which calculates the PSD from the raw data.

Chapter 6

Conclusion

I would like to conclude on the results and performance of my laser and bring forward some ideas for future improvements.

The laser in Littrow configuration I built convinces because of its large mode-hop-free tuning range of > 15 GHz and a narrow linewidth in the 100 kHz range. This helps us to lock it to a reference cavity or a spectroscopy cell to improve its performance. Also the long-term stable temperature control as well as the low-noise mechanical design [1] leads to a simple practical application in the experiment because the center linewidth observed on the wavemeter was almost not drifting over a long time so that once the grating arm was in its final position, it did not have to be realigned within at least four weeks.

In the last chapter I presented two methods to characterize the linewidth of the laser. Both results state a linewidth in the 100 kHz range where the cavity measurement gives a slightly broader spectral width. Reasons for this discrepancy were discussed. To verify the linewidth in the future, I recommend to use a reference cavity with a higher finesse. For the beatnote method the lasers should also be locked to minimize errors due to drifts of the lasers. In general, the second heterodyne method is the better technique because it represents the more realistic picture of the laser's linewidth and no model of the spectral distribution has to be assumed.

Since our group has now built two Littrow lasers of this type, problems and their solutions were investigated such that the setup of the same design should be straightforward. If a more narrow linewidth is desired, it could be considered to use not the 2 cm cavity length design but the one with 10 cm length for which a decrease of the linewidth by a factor of more than 20 is expected for 689 nm [1]. The output power I could reach is ≈ 22.5 mW which is in accordance with the datasheet of the laser diode. If more output power is required, a different laser diode for the 689 nm could be chosen next time. However, there are no laser diodes for 689 nm that have such a high quality anti-reflective coating than the one we use, which supports a large mode-hop-free tuning range and stable running conditions.

Acknowledgments

First, I would like to thank Sebastian Blatt for the amount of knowledge I was allowed to learn within ten weeks. You are a pool of ideas and your know-how is incredible. Getting things explained from you cannot be replaced by any textbook. Your engagement to teach me a good style of scientific writing, I appreciate a lot. Thank you!

Thanks, to Immanuel Bloch who did not only give me the opportunity to do my Bachelor's project in his group but also gives me the chance to go abroad for an internship. Your atomic physics lectures were inspiring to me and your enthusiasm infects all of your students, what I can say for sure.

I also would like to thank the whole strontium lab: Stephan for the nice introduction to the work in a lab and especially for his nerves because of all my questions. Annie who is the most helpful person and knows the lab as it would be her home. André for sharing his well-founded knowledge in physics and his humor with me. Stepan who was always my joker for software questions. Fabian for the nice talks during lunchtime. And Etienne for not burning *my* fingers during soldering.

Bibliography

- [1] E. C. Cook, P. J. Martin, T. L. Brown-Heft, J. C. Garman, and D. A. Steck. “High passive-stability diode-laser design for use in atomic-physics experiments”. In: *Review of Scientific Instruments* 83.043101 (2012). DOI: 10.1063/1.3698003.
- [2] T. H. Maiman. “Stimulated Optical Radiation in Ruby”. In: *Nature* 187 (1960), pp. 493–494. DOI: 10.1038/187493a0.
- [3] T. W. Hänsch and A. L. Schawlow. “Cooling of Gases by Laser Radiation”. In: *Optics Communication* 13.1 (1975), pp. 68–69. DOI: 10.1016/0030-4018(75)90159-5.
- [4] H. J. Metcalf and P. v. d. Straten. *Laser Cooling and Trapping*. Springer, 1999. ISBN: 978-1-4612-1470-0.
- [5] W. Ketterle and J. R. Anglin. “Bose-Einstein condensation of atomic gases”. In: *Nature* 416 (2002), pp. 211–218. DOI: 10.1038/416211a.
- [6] I. Bloch. “Ultracold quantum gases in optical lattices”. In: *Nature* 416 (2002), pp. 211–218. DOI: 10.1038/416211a.
- [7] I. Bloch, M. Greiner, O. Mandel, T. Esslinger, and T. W. Hänsch. “Quantum phase transition from a superfluid to a Mott insulator in a gas of ultracold atoms”. In: *Nature* 415 (2002), pp. 39–44. DOI: 10.1038/415039a.
- [8] X. Xu, T. H. Loftus, J. L. Hall, A. Gallagher, and J. Ye. “Cooling and trapping of atomic strontium”. In: *J. Opt. Soc. Am. B* 20.5 (2003). DOI: 10.1364/JOSAB.20.000968.
- [9] A. Einstein. “Strahlungs-Emission und -Absorption nach der Quantentheorie”. In: *Deutsche Physikalische Gesellschaft. Verhandlungen* 18 (1916), pp. 318–323.
- [10] C. J. Foot. *Atomic physics*. 1st ed. Oxford Master Series in Atomic, Optical, and Laser Physics. Oxford University Press, 2005. ISBN: 978-0-19-850696-6.
- [11] S. Hooker and C. Webb. *Laser Physics*. Oxford Master Series in Atomic, Optical, and Laser Physics. Oxford University Press, 2010. ISBN: 978-0-19-850692-8.

- [12] B.E.A. Saleh and M.C. Teich. *Fundamentals of Photonics*. 2nd ed. John Wiley & Sons, Inc., 2007. ISBN: 978-0-471-35832-9.
- [13] M. Balkanski and R. F. Wallis. *Semiconductor Physics and Applications*. Oxford University Press, 2000. ISBN: 978-0198517405.
- [14] R. Huebener. *Leiter, Halbleiter, Supraleiter*. 2nd ed. Springer, 2017. ISBN: 978-3-662-53280-5.
- [15] H. Ibach and H. Lüth. *Festkörperphysik*. 7th ed. Springer, 2009. ISBN: 978-3-540-85794-5.
- [16] W. Zinth and U. Zinth. *Optik*. 4th ed. Oldenburg Verlag, 2013. ISBN: 978-3-486-72136.
- [17] W. Wang, A. Major, and J. Palowal. “Grating-Stabilized External Cavity Diode Lasers for Raman Spectroscopy - A Review”. In: *Applied Spectroscopy Reviews* 47 (2012), pp. 116–142. DOI: 10.1080/05704928.2011.631649.
- [18] C. J. Hawthorn, K. P. Weber, and R. E. Scholten. “Littrow configuration tunable external cavity diode laser with fixed direction output beam”. In: *Review of Scientific Instruments* 72.12 (2001). DOI: 10.1063/1.1419217.
- [19] Steck Lab. University of Oregon. 2012. URL: <http://atomoptics-nas.uoregon.edu/unilaser/> (visited on 06/17/2017).
- [20] A. H. Mahvi. “Application of Ultrasonic Technology for Water and Wastewater Treatment”. In: *Iranian Journal of Public Health* 38 (2009).
- [21] URL: <https://refractiveindex.info/?shelf=glass&book=SCHOTT-BK&page=N-BK7> (visited on 06/17/2017).
- [22] C. Tanguy. “Temperature dependence of the refractive index of direct band gap semiconductors near the absorption threshold: Application to GaAs”. In: *Journal of Applied Physics* 80 (1996), pp. 4626–4631. DOI: 10.1063/1.363445.
- [23] N. Janša. “A frequency-stable diode laser system for spectroscopy and trapping of Sr atoms”. Master’s Thesis. LMU Munich, 2016. URL: http://ultracold.sr/theses/thesis_nejc_jansa.pdf.
- [24] J. G. Ziegler and N. B. Nichols. “Optimum Settings for Automatic Controllers”. In: *ASME* 64 (1942), pp. 759–768.
- [25] K. J. Åström and R. M. Murray. *Feedback Systems. An Introduction for Scientists and Engineers*. Princeton University Press, 2012. ISBN: 978-0-691-13576-2.
- [26] H. Kogelnik and T. Li. “Laser Beams and Resonators”. In: *Applied Optics* 5.10 (1966), pp. 1550–1567. DOI: 10.1364/AO.5.001550.

- [27] M. de Labachellerie and G. Passedat. “Mode-hop suppression of Littrow grating-tuned lasers”. In: *Applied Optics* 32.3 (1993), pp. 269–274. DOI: 10.1364/AO.32.000269.
- [28] Jérôme Lodewyck. Software “GaussianBeam” available online for free.
- [29] L. D. Turner, K. P. Weber, C. J. Hawthorn, and R. E. Scholten. “Frequency noise characterisation of narrow linewidth diode lasers”. In: *Optics Communications* 201.4-6 (2002), pp. 391–397. DOI: 10.1016/S0030-4018(01)01689-3.
- [30] C. A. DiMarzio. *Optics for Engineers*. CRC Press, 2012. ISBN: 978-1-4398-0725-5.

Appendix

A Calculations for Chapter 2.5

First, the Fourier transform of the single groove transmission function of the grating.:

$$\begin{aligned}
 \mathcal{F}[\Omega_{\text{groove}}(\xi)] &= \int_{-\infty}^{+\infty} \int_{-\infty}^{+\infty} \Omega_{\text{groove}}(\xi) \exp[-i((k_x - k_{x,0})\xi + (k_y - k_{y,0})\eta)] d\xi d\eta \\
 &= 2\pi\delta(k_y - k_{y,0}) \int_{-b/2}^{+b/2} \exp[-i(k_x - k_{x,0})\xi] d\xi \\
 &= 2\pi\delta(k_y - k_{y,0}) \frac{1}{-i(k_x - k_{x,0})} \left\{ \exp[-i(k_x - k_{x,0})b/2] - \exp[+i(k_x - k_{x,0})b/2] \right\} \\
 &= 2\pi\delta(k_y - k_{y,0}) \frac{2}{k_x - k_{x,0}} \sin[(k_x - k_{x,0})b/2].
 \end{aligned}$$

We use Eqn. (2.21), take the absolute value squared and ignore the δ -function in the y -direction to obtain:

$$I_{\text{groove}}(\theta, \theta_0) \propto \left| \mathcal{F}[\Omega_{\text{groove}}(\xi)] \right|^2 \propto \left\{ \frac{\lambda}{\pi(\sin \theta - \sin \theta_0)} \sin \left[\frac{\pi b}{\lambda} (\sin \theta - \sin \theta_0) \right] \right\}^2.$$

We normalize the intensity by the value at the coordinate origin. With $x := \sin \theta - \sin \theta_0$, we find

$$\begin{aligned}
 \lim_{x \rightarrow 0} I_{\text{groove}}(x) &\stackrel{2 \times \text{H\^opital's rule}}{\propto} b^2 \\
 \Rightarrow \frac{I_{\text{grooves}}(x)}{I_{\text{grooves}}(0)} &= \left[\frac{\lambda}{\pi b x} \sin \left(\frac{\pi b x}{\lambda} \right) \right]^2 = \text{sinc}^2 \left(\frac{\pi b x}{\lambda} \right).
 \end{aligned}$$

To find the intensity distribution of an grating with infinitely small grooves,

we use the Fourier transform of a δ -comb with N peaks in distance a :

$$\begin{aligned}\mathcal{F}[\Omega_{\text{comb}}(\xi)] &= \int_{-\infty}^{+\infty} \int_{-\infty}^{+\infty} \Omega_{\text{comb}}(\xi) \exp \left\{ -i [(k_x - k_{x,0})\xi + (k_y - k_{y,0})\eta] \right\} d\xi d\eta \\ &= 2\pi\delta(k_y - k_{y,0}) \sum_{m=0}^{N-1} \int_{-\infty}^{+\infty} \delta(\xi - ma) \exp(-i(k_x - k_{x,0})\xi) d\xi \\ &= 2\pi\delta(k_y - k_{y,0}) \sum_{m=0}^{N-1} \exp[-i(k_x - k_{x,0})ma]\end{aligned}$$

We use $\sum_{m=0}^n q^m = \frac{1-q^{n+1}}{1-q}$, ignore the δ -function again and set $x := \sin\theta - \sin\theta_0$ to find

$$\begin{aligned}\sum_{m=0}^{N-1} \exp\left(-i\frac{2\pi}{\lambda}max\right) &= \frac{1 - \exp(-i\frac{2\pi}{\lambda}Nax)}{1 - \exp(-i\frac{2\pi}{\lambda}ax)} \\ &= \frac{\exp(-i\frac{\pi}{\lambda}Nax) [\exp(+i\frac{\pi}{\lambda}Nax) - \exp(-i\frac{\pi}{\lambda}Nax)]}{\exp(-i\frac{\pi}{\lambda}ax) [\exp(+i\frac{\pi}{\lambda}ax) - \exp(-i\frac{\pi}{\lambda}ax)]} \\ &= \frac{\exp(-i\frac{\pi}{\lambda}Nax) \sin(\frac{\pi}{\lambda}Nax)}{\exp(-i\frac{\pi}{\lambda}ax) \sin(\frac{\pi}{\lambda}ax)}.\end{aligned}$$

The intensity is proportional to the absolute value squared, which is why the exponential function evaluates to unity. We get

$$I_{\text{comb}}(x) \propto \left[\frac{\sin(\frac{\pi}{\lambda}Nax)}{\sin(\frac{\pi}{\lambda}ax)} \right]^2.$$

Again we normalize the intensity to the value at the origin $I_{\text{comb}}(x=0)$ and obtain

$$\begin{aligned}\lim_{x \rightarrow 0} I_{\text{comb}}(x) &\stackrel{2 \times \text{H\^opital's rule}}{\propto} N^2 \\ \Rightarrow \frac{I_{\text{comb}}(x)}{I_{\text{comb}}(0)} &= \left[\frac{\sin(\frac{\pi}{\lambda}Nax)}{N \sin(\frac{\pi}{\lambda}ax)} \right]^2\end{aligned}$$

B Protection Circuit

The protection circuit was designed by Nejc Janša at MPQ. The first page Fig. B.1 shows the current supply, the DC modulation part, the relay for shunting the laser diode, the unimplemented AC modulation part as well as the connection to the thermistor and Peltier elements. On the second page in Fig. B.2 you can see the amplifier for the photodiode. This amplifier requires a power supply of

± 12 V. Since the protection board is designed to be supplied by ± 15 V, there is an additional voltage regulator. The Schottky diodes for protection from wrong input voltage are also shown.

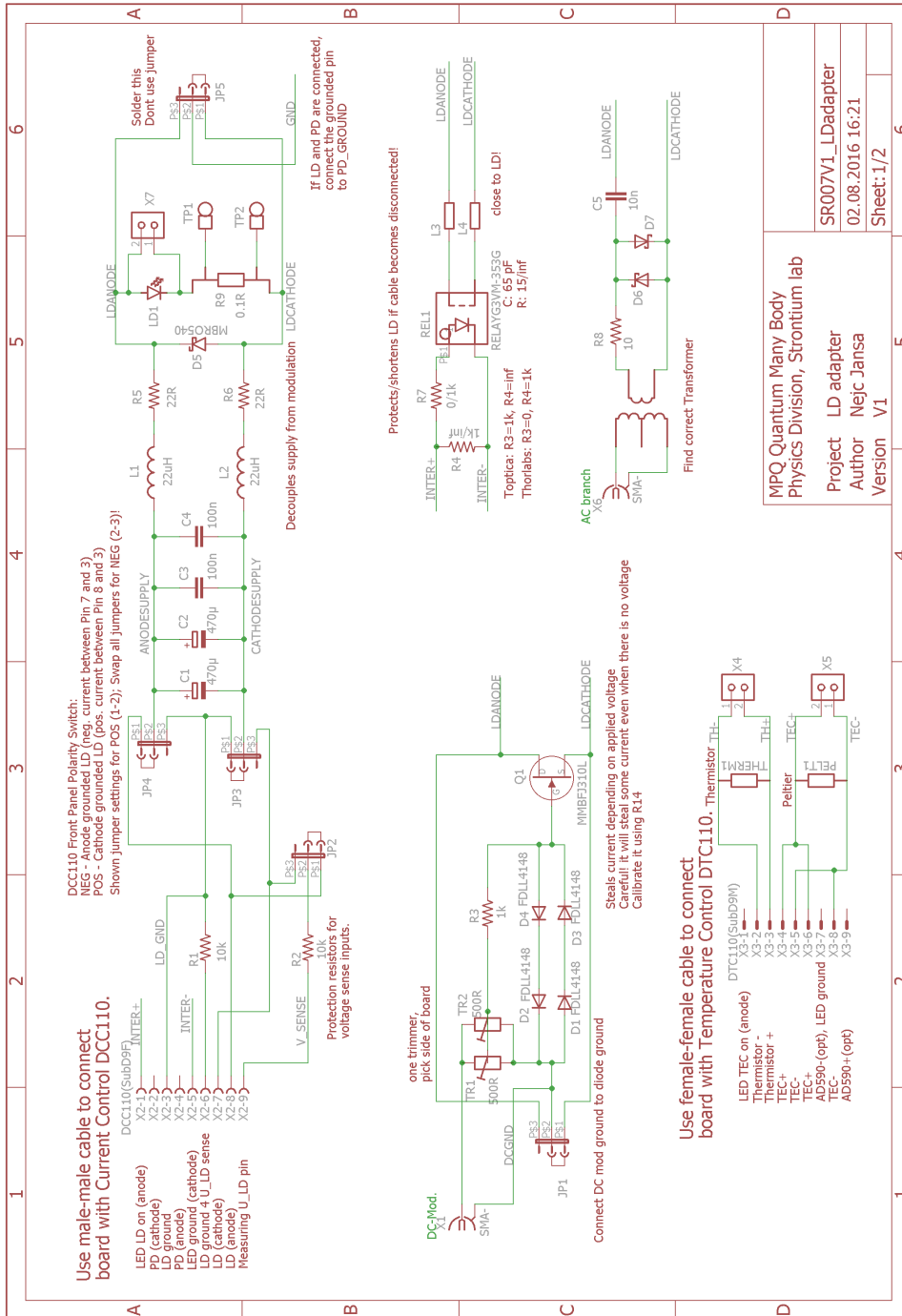
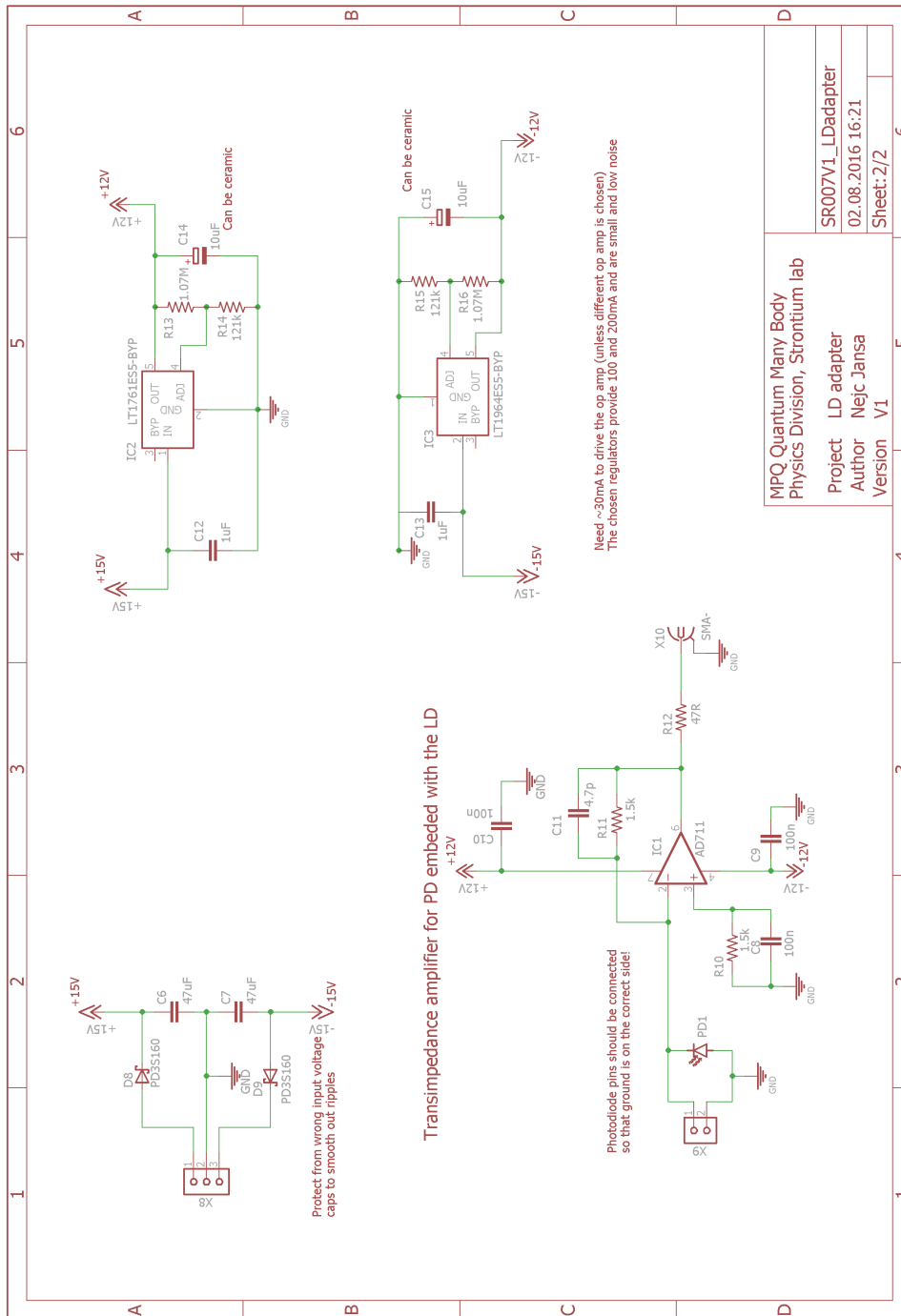


Figure B.1: The protection circuit page 1/2.



MPQ Quantum Many Body Physics Division, Strontium lab
Project LD adapter
Author Nejc Jansa
Version V1
SR007V1_LDadapter
02.08.2016 16:21
Sheet: 2/2

Figure B.2: The protection circuit page 2/2

C Magnification Factor of an Anamorphic Prism Pair

The angles of diffraction are connected by sine functions. In addition, the magnification M of a beam on one surface also depends on cosine functions. For this reason, the complete form of M gets complex. Nevertheless, I put my results here to save the reader from calculating this hideous equation. The angles are chosen as shown in Fig. 4.2b. Here, n describes the refractive index of the glass and β is the angle between the optical axis and the incoming beam.

$$\begin{aligned}
 M(\alpha_1, \alpha_2, \alpha, \beta, n) &= \sec(\alpha_1 + \beta) \sqrt{1 - \frac{\sin^2(\alpha_1 + \beta)}{n^2}} \\
 &\sqrt{1 - n^2 \sin^2 \left\{ \alpha - \sin^{-1} \left[\frac{\sin(\alpha_1 + \beta)}{n} \right] \right\}} \\
 &\sec \left\{ \alpha - \sin^{-1} \left[\frac{\sin(\alpha_1 + \beta)}{n} \right] \right\} \\
 &\sqrt{1 - \frac{\sin^2 \left\{ \alpha - \alpha_1 + \alpha_2 - \sin^{-1} \left[n \sin \left[\alpha - \sin^{-1} \left(\frac{\sin(\alpha_1 + \beta)}{n} \right) \right] \right] \right\}}{n^2}} \\
 &\sqrt{1 - n^2 \sin^2 \left\{ \alpha + \sin^{-1} \left\{ \frac{\sin \left[\alpha - \alpha_1 + \alpha_2 - \sin^{-1} \left[n \sin \left(\alpha - \sin^{-1} \left(\frac{\sin(\alpha_1 + \beta)}{n} \right) \right) \right] \right] \right\}}{n} \right\}} \right\} \\
 &\sec \left\{ \alpha - \alpha_1 + \alpha_2 - \sin^{-1} \left\{ n \sin \left[\alpha - \sin^{-1} \left(\frac{\sin(\alpha_1 + \beta)}{n} \right) \right] \right\} \right\} \\
 &\sec \left\{ \alpha + \sin^{-1} \left\{ \frac{\sin \left[\alpha - \alpha_1 + \alpha_2 - \sin^{-1} \left[n \sin \left(\alpha - \sin^{-1} \left(\frac{\sin(\alpha_1 + \beta)}{n} \right) \right) \right] \right] \right\}}{n} \right\} \right\} \\
 &\hspace{15em} (.2)
 \end{aligned}$$

The angle δ of the outgoing beam in relation to the optical axis is of importance because it is desired to have a minimal deviation from the initial beam path. Then, δ is given by

$$\begin{aligned}
 \delta(\alpha_1, \alpha_2, \alpha, \beta, n) &= -\alpha - \alpha_2 \\
 &+ \sin^{-1} \left\{ n \sin \left\{ \alpha + \sin^{-1} \left[\frac{\sin \left[\alpha - \alpha_1 + \alpha_2 - \sin^{-1} \left[n \sin \left(\alpha - \sin^{-1} \left(\frac{\sin(\alpha_1 + \beta)}{n} \right) \right) \right] \right] \right] \right\}}{n} \right\} \right\} \\
 &\hspace{15em} (.3)
 \end{aligned}$$

Hiermit erkläre ich, die vorliegende Arbeit selbständig verfasst zu haben und keine anderen als die in der Arbeit angegebenen Quellen und Hilfsmittel benutzt zu haben.

München, den 03. Juli 2017